Journal of Medicinal Chemistry

Article

pubs.acs.org/jmc

Exploring the Directionality of 5-Substitutions in a New Series of 5-Alkylaminopyrazolo[4,3-*e*]1,2,4-triazolo[1,5-*c*]pyrimidine as a Strategy To Design Novel Human A_3 Adenosine Receptor Antagonists.

Stephanie Federico,[†] Antonella Ciancetta,[‡] Davide Sabbadin,[‡] Silvia Paoletta,[‡] Giorgia Pastorin,[§] Barbara Cacciari,[⊥] Karl Norbert Klotz,[□] Stefano Moro,*[,‡] and Giampiero Spalluto*[,†]

[†]Dipartimento di Scienze Chimiche e Farmaceutiche, Università di Trieste, Piazzale Europa 1, I-34127 Trieste, Italy

[‡]Molecular Modeling Section (MMS), Dipartimento di Scienze del Farmaco, Università di Padova, via Marzolo 5, I-35131 Padova, Italy

[§]Department of Pharmacy, National University of Singapore, 3 Science Drive 2, Singapore 117543

[⊥]Dipartimento di Scienze Farmaceutiche, Università degli Studi di Ferrara, via Fossato di Mortara 17-19, I-44100 Ferrara, Italy

[□]Institut für Pharmakologie, Universität of Würzburg, D-97078 Würzburg, Germany

Supporting Information

ABSTRACT: The structure−activity relationship (SAR) of new 5-alkylaminopyrazolo-[4,3-*e*]1,2,4-triazolo[1,5-*c*]pyrimidines as antagonists of the A_3 adenosine receptor (AR) was explored with the principal aim to establish the directionality of 5-substitutions inside the orthosteric binding site of the A_3 AR. All the synthesized compounds showed affinity for the hA_3 AR from nanomolar to subnanomolar range. In particular, the most potent and selective antagonist presents an (*S*) *α*-phenylethylamino moiety at the 5 position (**26**, K_i hA_3 = 0.3 nM). Using an in silico receptor-driven approach, we have determined the most favorable orientation of the substitutions at the 5 position of the pyrazolo[4,3-*e*]1,2,4-triazolo[1,5-*c*]-pyrimidine (PTP) scaffold, opening the possibility for further derivatizations aimed at directing the N^5 position toward the extracellular environment.

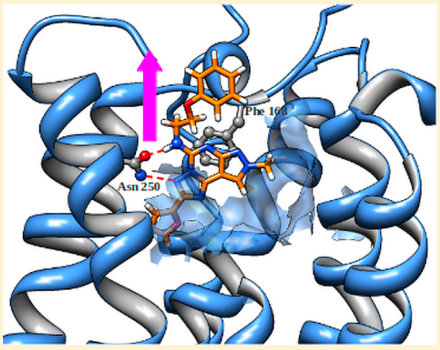

INTRODUCTION

Adenosine is a neuromodulator exerting several functions through the activation of specific G protein-coupled receptors that are classified into four different subtypes, termed A_1, A_{2A}, A_{2B}, and A_3, based on pharmacological criteria and coupling to adenylyl cyclase.[1,2] The adenosine A_3 receptor (A_3 AR) was first cloned from a rat testis cDNA library[3] and is still undergoing intensive pharmacological characterization. Subsequently, A_3 ARs have also been cloned from several other species such as human,[4,5] sheep,[6] mouse,[7] and rabbit.[8] However, significant differences in sequence similarity (72%) have been detected among different species:[9,10] The rat A_3 adenosine receptor (rA_3 AR), especially, behaves anomalously in ligand binding assays.[11]

The activation of A_3 ARs is related to various second messenger systems: In particular, they have been shown to stimulate phospholipase C[12] and D[13] and to inhibit adenylyl cyclase.[14] In the rat, the activation of A_3 ARs results in hypotension through the promotion of the release of inflammatory mediators from mast cells.[15] It has also been suggested that the A_3 AR plays an important role in brain ischemia,[16] immunosuppression,[17] and cellular growth.[18]

On the basis of these pharmacological observations, many efforts have been made in search of highly selective A_3 AR antagonists as potential antiasthmatic,[19] antinflammatory, and cerebroprotective agents and for the treatment of glaucoma.[9,20,21] For this purpose, in the past few years, different classes of heterocyclic derivatives have emerged as A_3 AR antagonists.[22]

In this research field, our group has reported a large series of pyrazolo[4,3-*e*]1,2,4-triazolo[1,5-*c*]pyrimidine (PTP) derivatives as highly potent and selective human A_3 adenosine receptor (hA_3 AR) antagonists.[23−28] In particular, we observed that the simultaneous introduction of a methyl group at the N^8 position and the presence of aryl carbamoyl (**1**) or arylacetyl (**2**) moieties at the N^5 position led to potent and selective hA_3 AR antagonists (Chart 1).[23−25]

In addition, we have recently reported a novel series of PTP-based fluorophore-conjugated hA_3 AR antagonists with a versatile application in cell-based assay ligand discovery and receptor localization imaging.[29] Herein, we report the essential pilot work based on an extensive exploration of new possible spacers at the N^5 position as a site of linkage not only for fluorophore groups but also for other possible functionalizing moieties that can be useful in the study of the physiological and

Received: June 26, 2012
Published: October 25, 2012

   dx.doi.org/10.1021/jm300899q | *J. Med. Chem.* 2012, 55, 9654−9668

Chart 1. Arylcarbamoyl and Arylacetyl Pyrazolo-triazolo-pyrimidine Derivatives as Human A_3 Adenosine Receptor Antagonists

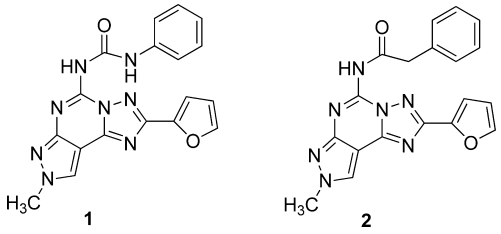

physiopathological roles of ARs. We focused on substituents of different natures and sizes, to evaluate their ability to direct the N^5 position toward the extracellular environment.

To this aim, we decided to modify the synthetic approach to the PTP nucleus (see Chemistry): The new approach has enabled us to introduce a large variety of polyfunctionalized chains, such as alkoxy or alkyl amino moieties, at the 5 position under mild conditions, leading to the design and synthesis of compounds **3**–**62** (Chart 2). Along with the pharmacological

Chart 2. General Structures of Synthesized Compounds 3–62

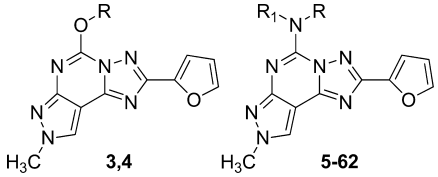

evaluation, the new derivatives have also been subjected to molecular modeling studies, to better analyze the essential structural requirements to direct the N^5 position toward the extracellular environment, while retaining both affinity and selectivity at the hA_3 AR. Therefore, the new derivatives herein reported may help in the design and development of new potent hA_3 AR antagonists as well as linkage points for functionalizing groups aimed at the study of ARs functions.

RESULTS AND DISCUSSION

A. Chemistry. All the designed compounds **3**–**62** have been synthesized as summarized in Scheme 1. By reacting the well-known triazolylpyrazolamino derivative **63**[24] with diphosgene in dry dioxane, the corresponding cyclized derivative **64** was obtained. The latter, after treatment with a mixture of $POCl_3/PCl_5$ in pyridine, afforded the chloro derivative **65** which, after reaction with sodium ethoxide or methoxide in dry ethanol or methanol at reflux, gave the corresponding alkyloxy derivatives **3** and **4**. Instead, by reacting the chloro derivative **65** with an appropriate alkyl- or aralkylamine in ethanol in a sealed tube at 110 °C, the corresponding 5-(ar)alkylamino derivatives **5**–**62** were obtained.

B. Biological Activity. The newly synthesized compounds (**3**–**62**, **64**, **65**) were tested at the human A_1, A_{2A}, and A_3 receptors expressed in CHO cells: [^{3}H]CCPA (A_1) and [^{3}H]NECA (A_{2A}, A_3) were used as radioligands in binding assays.[30] As far as the activity at the human A_{2B} AR is concerned, the inhibition of NECA-stimulated adenylyl cyclase activity was determined as a measurement of the affinity of the compounds.

Structure–Activity Relationships. As clearly summarized in Table 1, all the synthesized compounds (**3**–**62**, **64**, **65**) showed affinities at the hA_3 AR ranging from high nanomolar to sub-nanomolar concentrations, with different degree of selectivity versus hA_1 AR and hA_{2A} AR, while being almost inactive at the hA_{2B} AR. It is quite evident that compounds lacking the amino group at the 5 position (**3**, **64**, **65**) exhibit low affinity at the hA_3 AR. An exception is represented by compound **4** bearing an ethoxy moiety at the 5 position, which possesses quite good affinity (hA_3 AR K_i = 182 nM) but low levels of selectivity versus the other receptor subtypes.

A significant recovery of the affinity at the hA_3 AR can be observed with the 5-alkylamino derivatives (**5**–**62**). A detailed analysis of binding data has clearly revealed the effect of the substituent at the N^5 position on the hA_3 AR affinity and selectivity. In particular, small alkyl groups such as methyl (**5**) or ethyl (**6**) give pretty good affinity at the hA_3 AR (hA_3 AR K_i = 63.3 nM and hA_3 AR K_i = 44.4 nM, respectively), but the

Scheme 1[a]

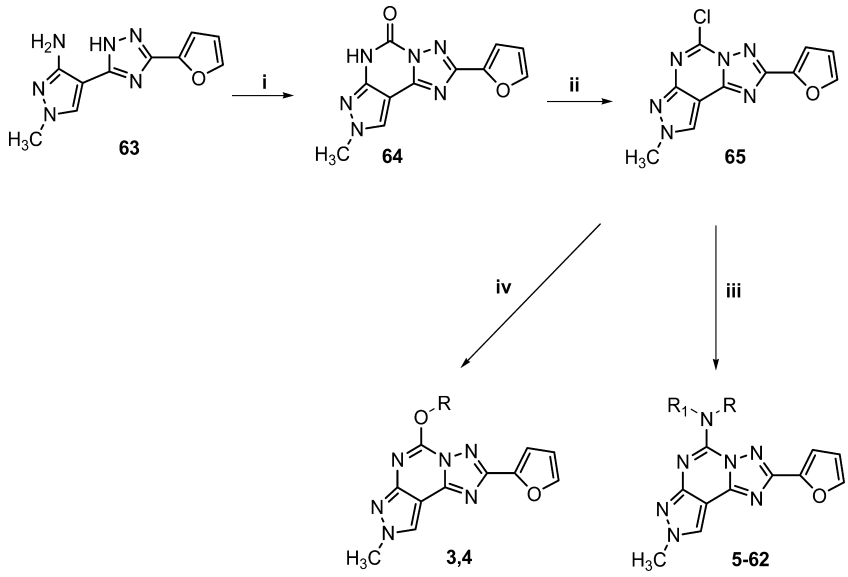

[a]Reagents and conditions: (i) Diphosgene, dry dioxane, 70 °C, 90 min; (ii) $POCl_3/PCl_5$, dry pyridine, reflux, 24 h; (iii) RONa, ROH, reflux, 2 h; (iv) R_1RNH, EtOH, 110 °C, sealed tube, 2 h.

dx.doi.org/10.1021/jm300899q | J. Med. Chem. 2012, 55, 9654–9668

Table 1. Structures and Binding Profile of Synthesized Compounds 3−62, 64, and 65

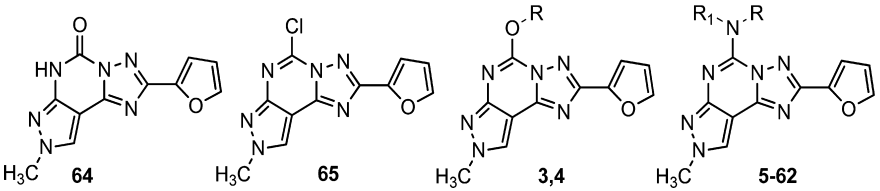

compd	R	R_1	hA_1 (K_i, nM)[a]	hA_{2A} (K_i, nM)[b]	hA_{2B} (K_i, nM)[c]	hA_3 (K_i, nM)[d]	hA_1/hA_3	hA_{2A}/hA_3	hA_1/hA_{2A}
64	–	–	>30000	>30000	>10000	5280 (4220−6610)	>5.68	>5.68	–
65	–	–	6560 (5440−7910)	29900 (21300−42100)	>10000	367 (306−441)	17.9	81.5	0.22
3	CH_3	–	>30000	>30000	>10000	822 (757−893)	>36.5	>36.5	–
4	CH_2CH_3	–	7750 (5790−9880)	6120 (5240−7140)	>10000	182 (135−245)	42.6	33.6	1.27
5	CH_3	H	1930 (1620−2300)	368 (213−636)	2110 (1700−2610)	63.4 (56.0−71.9)	30.4	5.8	5.24
6	CH_2CH_3	H	604 (476−765)	208 (124−352)	2160 (2110−2210)	44.4 (29.8−66.2)	13.6	4.68	2.9
7	$CH(CH_3)_2$	H	333 (283−390)	389 (296−511)	9720 (6250−15100)	34.1 (25.6−45.5)	9.76	11.4	0.86
8	$CH(CH_3)CH_2CH_3$ (*R*,*S*)	H	131 (91.9−187)	248 (152−405)	3860 (2570−5770)	5.23 (4.11−6.66)	25	47.4	0.53
9	$CH(CH_3)CH_2CH_3$ (*S*)	H	129 (112−149)	244 (177−337)	2600 (1970−3430)	11.0 (6.69−18.0)	11.7	22.2	0.53
10	$CH(CH_3)CH_2CH_3$ (*R*)	H	165 (130−209)	272 (154−483)	4810 (3300−7020)	5.93 (5.10−6.90)	27.8	45.9	0.61
11	*n*-C_5H_{11}	H	481 (420−550)	168 (95.5−295)	3980 (2410−6450)	14.6 (10.5−20.4)	32.9	11.5	2.86
12	$CH(CH_3)(CH_2)_4CH_3$	H	248 (236−260)	446 (311−640)	7660 (5450−10700)	8.62 (6.00−12.4)	28.8	51.7	0.56
13	$CH(CH_3)(CH_2)_5CH_3$	H	265 (150−469)	701 (427−1150)	>10000	23.8 (22.1−25.5)	11.1	29.4	0.38
14	$CH_2CH(CH_2CH_3)(CH_2)_3CH_3$	H	605 (540−679)	512 (340−770)	>10000	3.82 (3.01−4.85)	158	134	1.18
15	$C(CH_3)_2C(CH_3)_3$	H	982 (910−1060)	3230 (2120−4940)	>10000	130 (101−168)	7.55	24.8	0.30
16	c-C_3H_5	H	208 (187−232)	113 (104−124)	1750 (1120−2740)	69.3 (53.0−90.6)	3	1.63	1.84
17	c-C_4H_7	H	169 (129−221)	83.9 (69.9−101)	1110 (869−1410)	17.6 (15.9−19.4)	9.6	4.77	2.01
18	c-C_5H_9	H	80.1 (63.9−100)	130 (105−162)	2650 (1730−4040)	7.68 (4.43−13.3)	10.4	16.9	0.62
19	c-C_6H_{11}	H	166 8147−186)	233 (170−320)	6320 (4200−9460)	8.57 (7.73−9.50)	19.4	27.2	0.71
20	c-C_7H_{13}	H	223 (177−282)	336 (233−483)	6590 (5070−8530)	15.4 (8.98−26.3)	14.5	21.8	0.66
21	c-C_8H_{15}	H	484 (472−496)	279 (214−363)	>10000	15.5 (8.49−28.1)	31.2	18	1.73
22	CH_2-c-C_6H_{11}	H	802 (709−908)	814 (682−972)	9650 (8980−10200)	47.3 (32.4−68.9)	17	17.2	0.98
23	1-adamantyl	H	3310 (2010−5460)	>30000	>10000	37.8 (28.6−50.1)	87.6	>794	-
24	2-adamantyl	H	750 (410−1370)	848 (327−2200)	>10000	18.8 (17.9−19.8)	39.9	45.1	0.88
25	CH_2Ph	H	527 (438−634)	91.0 (40.8−203)	3330 (2460−4550)	2.49 (2.36−2.63)	212	36.5	5.79
26	$CH(CH_3)Ph$ (*S*)	H	338 (293−391)	55.2 (28.7−106)	5290 (4100−6800)	0.30 (0.21−0.42)	1127	184	6.12
27	$CH(CH_3)Ph$ (*R*)	H	945 (780−1150)	38.2 (29.8−48.9)	12200 (8400−17700)	3.71 (2.72−5.05)	255	10.3	24.7
28	CH_2Ph-4-CH_3	H	538 (447−648)	117 (93−148)	3940 (1890−8300)	1.07 (0.73−1.55)	503	109	4.6
29	CH_2Ph-4-OCH_3	H	442 (382−512)	177 (148−212)	9840 (7760−12500)	6.92 (4.51−10.6)	63.9	25.6	2.5
30	CH_2Ph-4-Cl	H	322 (318−325)	75.4 (61.9−91.8)	2620 (2130−3240)	1.99 (1.80−2.19)	162	37.9	4.27
31	CH_2Ph-4-F	H	823 (589−1150)	87.5 (81.3−94.1)	3180 (1580−6410)	4.93 (4.29−5.66)	167	17.8	9.41
32	CH_2Ph-4-CF_3	H	1230 (1120−1360)	245 (165−362)	>3000	14.9 (13.4−16.5)	82.5	16.4	5.02
33	CH_2Ph-3,4-$(OCH_3)_2$	H	2720 (1910−3890)	64.1 (49.5−82.9)	>3000	21.1 (18.9−23.6)	129	3.04	42.3
34	CH_2Ph-4-Ph	H	17500 (10300−29900)	593 (532−660)	>10000	187 (150−233)	93.6	3.17	29.5
35	$CHPh_2$	H	169 (159−181)	900 (664−1220)	>10000	0.83 (0.76−0.92)	204	1084	0.19

dx.doi.org/10.1021/jm300899q | J. Med. Chem. 2012, 55, 9654−9668

Table 1. continued

compd	R	R_1	hA_1 (K_i, nM)[a]	hA_{2A} (K_i, nM)[b]	hA_{2B} (K_i, nM)[c]	hA_3 (K_i, nM)[d]	hA_1/hA_3	hA_{2A}/hA_3	hA_1/hA_{2A}
36	CH_2CH_2Ph	H	733 (656−820)	46.1 (28.5−74.6)	2790 (1650−4710)	52.8 (52.2−53.4)	13.9	0.87	15.9
37	CH_2CH_2Ph-3,4-$(OCH_3)_2$	H	1580 (1120−2230)	92.5 (65.6−130)	3880 (2980−5070)	37.6 (27.5−51.4)	42	2.46	17.1
38	$CH(CH_3)CH_2CH_2Ph$	H	133 (88.2−199)	147 (128−170)	5260 (3560−7800)	37.8 (34.9−41.0)	3.52	3.89	0.9
39	CH_2CH_2-3-indolyl	H	1250 (781−1990)	77.0 (42.9−138)	2870 (2320−3530)	30.9 (27.7−34.4)	40.4	2.49	16.2
40	CH_2CH_2OH	H	649 (500−842)	157 (143−173)	7470 (6450−8660)	309 (271−353)	2.1	0.51	4.13
41	$CH_2CH_2CH_2OH$	H	212 (187−239)	155 (131−183)	9300 (7050−12300)	241 (163−355)	0.88	0.64	1.37
42	$CH_2CH(OH)CH_3$	H	375 (308−457)	136 (123−151)	>3000	356 (179−707)	1.05	0.38	2.76
43	$CH(CH_2CH_3)CH_2OH$	H	219 (165−292)	207 (187−228)	>10000	62.9 (41.5−95.3)	3.48	3.29	1.06
44	$CH(CH_2OH)_2$	H	639 (422−967)	597 (415−859)	>10000	536 (343−835)	1.19	1.11	1.07
45	$CH_2(CH_2)_2CH_2OH$	H	1040 (930−1170)	251 (215−293)	>10000	252 (176−360)	4.13	1	4.14
46	$CH_2(CH_2)_3CH_2OH$	H	525 (437−630)	124 (104−148)	>10000	136 (108−172)	3.86	0.91	4.23
47	$CH_2(CH_2)_4CH_2OH$	H	483 (406−574)	109 (77.3−155)	>10000	156 (141−172)	3.10	0.70	4.43
48	OCH_3	H	2750 (2050−3700)	185 (146−234)	8500 (6160−11700)	404 (368−442)	6.81	0.46	14.9
49	$CH_2CH_2OCH_3$	H	2400 (1580−3630)	407 (315−528)	>10000	246 (204−297)	9.76	1.65	5.90
50	CH_2CH_2OPh	H	646 (469−889)	121 (101−144)	7500 (5100−11100)	38.6 (32.5−46.0)	16.7	3.13	5.34
51	CH_3	CH_3	4760 (2830−8010)	1030 (844−1250)	>10000	394 (343−453)	12.1	2.61	4.62
52	CH_3	$CH_2(CH_2)_2CH_3$	1060 (931−1220)	1380 (1260−1510)	>10000	36.7 (31.3−43.0)	28.9	37.6	0.77
53	CH_2CH_3	CH_2CH_3	1450 (1280−1650)	798 (426−1500)	>10000	96.3 (61.7−150)	15.1	8.29	1.82
54	$CH_2(CH_2)_3CH_3$	$CH_2(CH_2)_3CH_3$	3330 (3090−3590)	7490 (6270−8960)	>10000	824 (639−1060)	4.04	9.09	0.44
55	CH_3	cC_6H_{11}	1020 (777−1330)	2730 (2380−3130)	>10000	32.7 (22.5−47.5)	31.2	83.5	0.37
56	CH_3	CH_2Ph	566 (481−668)	1080 (719−1620)	>10000	18.0 (16.1−20.2)	31.4	60	0.52
57	CH_2Ph	CH_2Ph	711 (658- $CH_3$768)	1150 (743−1770)	>10000	404 (349−467)	1.76	2.85	0.62
58	CH_2CH_3	CH_2CH_2OH	15000 (13400−16700)	6430 (6120−6760)	>10000	1360 (732−2540)	11	4.73	2.33
59	–	*N*-pyrrolidinyl	328 (262−409)	132 (81.0−215)	>10000	35.5 (29.3−43.1)	9.24	3.72	2.48
60	–	*N*-piperidinyl	2150 (1580−2910)	352 (258−481)	>10000	38.1 (19.5−74.3)	56.4	9.24	6.11
61	–	4-methyl-1-piperazinyl	15200 (13500−17100)	7690 (4660−12700)	>10000	1330 (1030−1730)	11.4	5.78	1.98
62	–	4-morpholinyl	2420 (1970−2990)	1670 (1070−2600)	>10000	514 (469−563)	4.71	3.25	1.45

[a]Displacement of specific [^{3}H]-CCPA binding at human A_1 receptors expressed in CHO cells (n = 3−6). [b]Displacement of specific [^{3}H]-NECA binding at human A_{2A} receptors expressed in CHO cells. [c]K_i values of the inhibition of NECA-stimulated adenylyl cyclase activity in CHO cells expressing hA_{2B} receptors. [d]Displacement of specific [^{3}H]-NECA binding at human A_3 receptors expressed in CHO cells. Data are expressed as geometric means, with 95% confidence limits.

dx.doi.org/10.1021/jm300899q | J. Med. Chem. 2012, 55, 9654−9668

levels of selectivity are still poor. Interestingly, elongation of the chain at the N^5 position increases the affinity (e.g., compound **11**, hA_3 AR K_i = 14.6 nM) but without selectivity versus the other receptor subtypes.

Branched chains such as *sec*-butyl (**8**) also significantly increase the affinity at the hA_3 AR with an acceptable selectivity (hA_1/hA_3 = 25; hA_{2A}/hA_3 = 47). By implementing the lipophilic character of the chain at the N^5 position (e.g., compound **14**), both affinity and selectivity are significantly increased (hA_3 AR K_i = 3.82 nM; hA_1/hA_3 = 158; hA_{2A}/hA_3 = 134), whereas the introduction of bulky substituents (e.g., compound **15**) reduces both the affinity and the selectivity (hA_3 AR K_i = 130 nM; hA_1/hA_3 = 7.5; hA_{2A}/hA_3 = 25). A similar behavior can be observed with the introduction of cycloalkyl substituents at the N^5 position. In general, all the cycloalkyl amino derivatives (**16**−**22**) show good affinity at the hA_3 AR. In particular, a good affinity can be obtained by introducing five- (**18** hA_3 AR K_i = 7.68 nM) or six-membered rings (**19** hA_3 AR K_i = 8.57 nM), while smaller (e.g., **16** hA_3 AR K_i = 69.3 nM) or larger (e.g., **20** hA_3 AR K_i = 15.4 nM) rings lead to a significant reduction of the affinity. However, bulky substituents, such as the c-octyl (**21**) and 2-adamantyl (**24**) moieties, are more tolerated than the smaller cyclopropyl (**16**) group (**21** hA_3 AR K_i =15.5 nM, **24** hA_3 AR K_i =18.8 nM vs **16** hA_3 AR K_i =69.3 nM). Also the selectivity versus the other receptor subtypes increases from the cyclopropyl (**16**: hA_1/hA_3 = 3; hA_{2A}/hA_3 = 1.63) to the cyclohexyl (**19**: hA_1/hA_3 = 19.4; hA_{2A}/hA_3 = 27.2) derivatives, but generally the levels of selectivity are very low.

In the cycloalkylamino series, the two adamantyl derivatives **23** and **24** show completely different binding profiles: In fact, while the 2-isomer (**24**) is more potent at the hA_3 AR (hA_3 AR K_i = 18.8 nM vs hA_3 AR K_i = 37.8 nM for **24** and **23**, respectively), the selectivity profile versus the other receptor subtypes is the exact opposite (**23**: hA_1/hA_3 = 87; hA_{2A}/hA_3 = >794; **24**: hA_1/hA_3 = 39.9; hA_{2A}/hA_3 = 45.1).

Introduction of a benzyl group at the N^5 position (**25**) leads to an improvement of the affinity at the hA_3 AR with good levels of selectivity (hA_3 AR K_i = 2.5 nM; hA_1/hA_3 = 212; hA_{2A}/hA_3 = 36.5). Substitutions on the phenyl ring seems not to have significant effects on both the hA_3 AR affinity and selectivity, with the exception of the 4-methyl derivative (**28**), which displays increased affinity and selectivity (hA_3 AR K_i = 1.07 nM; hA_1/hA_3 = 503; hA_{2A}/hA_3 = 109). Conversely, the presence of a 4-CF_3 (**32**), 4-Ph (**34**), or phenyl disubstitutions (**33**) is detrimental in terms of affinity and selectivity (e.g., compound **34** hA_3 AR K_i = 187 nM; hA_1/hA_3 = 93; hA_{2A}/hA_3 = 3).

Substitution at the N^5 position with a β-phenylethyl moiety (**36**) also leads to a significant loss of affinity and selectivity (hA_3 AR K_i = 52.8 nM; hA_1/hA_3 = 13; hA_{2A}/hA_3 = 0.8), thus confirming that the presence of a carbonyl group such as in the reference compound **2** plays a fundamental role in the receptor recognition as previously reported.[22−27] Nevertheless, the data reported in Table 1 suggest that the introduction of additional hydrophobic groups might balance the carbonyl lacking and allow the recovery of the affinity. In fact, the benzhydryl derivative **35** shows a K_i value at the hA_3 AR of 0.83 nM and high levels of selectivity versus the other receptor subtypes (hA_1/hA_3 = 204; hA_{2A}/hA_3 = 1084). Also with an α-phenylethyl moiety at the N^5 position, a very potent and selective compound is obtained (**26**: hA_3 AR K_i = 0.3 nM; hA_1/hA_3 = 1,127; hA_{2A}/hA_3 = 184). Considering the α-phenylethyl substitution, it is quite evident the effect of the stereochemistry of the chain at the 5 position: the (*S*) isomer (**26**) is 10-fold more potent at the hA_3 AR than its (*R*) enantiomer (**27**) (**26**: hA_3 AR K_i = 0.3 nM; **27**: hA_3 AR K_i = 3.7 nM) with an improved selectivity as a consequence (**26**: hA_1/hA_3 = 1127; hA_{2A}/hA_3 = 184; **27**: hA_1/hA_3 = 255; hA_{2A}/hA_3 = 10.3). It should be otherwise noted that a similar effect of the stereochemistry has not been observed for derivatives **9** and **10**, suggesting that also the kind of substitution plays a fundamental role in the receptor recognition.

Further elongation of the spacer between the phenyl ring and the amino function (**37**, **38**) or its replacement with a heterocycle such as indole (**39**) significantly decreases the affinity and the selectivity at the hA_3 AR.

Further support that the increase of the liphophilic character might help in achieving activity at the hA_3 AR is suggested by the binding data of compounds **40**−**50**: In fact, the introduction of polar chains bearing hydroxyl functions at the N^5 position is detrimental for both the affinity and the selectivity (e.g., compound **44**: hA_3 AR K_i = 536 nM; hA_1/hA_3 = 1.2; hA_{2A}/hA_3 = 1.1), and only when the aliphatic chain is longer and/or branched is a partial recovery of the affinity observed, even though the selectivity still remains poor (e.g., compound **43**: hA_3 AR K_i = 62.9 nM; hA_1/hA_3 = 3.5; hA_{2A}/hA_3 = 3.3).

Moreover, etherification of the hydroxyl group permits, in part, affinity at the hA_3 AR but without significant selectivity. In particular, derivative **50**, bearing at the 5 position a phenoxyethyl amino group, shows quite good affinity at the hA_3 AR (K_i = 38.6 nM) but with low levels of selectivity versus the other receptor subtypes (hA_1/hA_3 = 16.7; hA_{2A}/hA_3 = 3.13). Disubstitutions of the nitrogen at the 5 position with small alkyl groups such as methyl (**51**) or ethyl (**53**) leads to a significant reduction of the affinity with consequent loss of selectivity (e.g., compound **51**: hA_3 AR K_i = 394 nM; hA_1/hA_3 = 12.1; hA_{2A}/hA_3 = 2.61). Nevertheless, if one of the substituents is a bulky group, such as *n*-butyl (**52**) or benzyl (**56**), an increase of both affinity and selectivity is observed (e.g., compound **56**: hA_3 AR K_i = 18 nM; hA_1/hA_3 = 31.4; hA_{2A}/hA_3 = 60), while the simultaneous introduction of two bulky substituents (e.g., compound **57**: hA_3 AR K_i = 404 nM; hA_1/hA_3 = 1.8; hA_{2A}/hA_3 = 2.9) or a presence of hydrophilic functions (e.g., compound **58**: hA_3 AR K_i = 1,360 nM; hA_1/hA_3 = 11; hA_{2A}/hA_3 = 4.7) dramatically reduces the affinity and the selectivity at the hA_3 AR.

Introduction of cyclic amines at the 5 position produces different effects on the binding profile depending on the nature of the heterocycle. While pyrrolidine (**59**) or piperidine (**60**) are well tolerated in terms of affinity (e.g., compound **59**: hA_3 AR K_i = 35.5 nM), the introduction of heterocycles with a protonable basic moiety at the 4 position such as piperazine (**61**) or morpholine (**62**) leads to a drastic reduction of the affinity at the hA_3 AR (e.g., compound **61**: hA_3 AR K_i = 1330 nM). Nevertheless, for all these derivatives (**59**−**62**), the selectivity versus the other receptor subtypes is very low.

C. Molecular Modeling. With the aim to rationalize from a molecular point of view the observed binding data, all the newly synthesized analogues have been subjected to a molecular modeling investigation. The new derivatives were docked into the binding cavity of the hA_3 AR with the aim to identify their hypothetical binding mode at this receptor subtype by focusing the attention on the orientation of the N^5 substituents. As, to date, no crystallographic information about the A_3 AR is available, we performed the docking studies by using a hA_3 AR homology model, which has been previously proposed[31] and built by using the crystal structure of the hA_{2A} AR[32] as

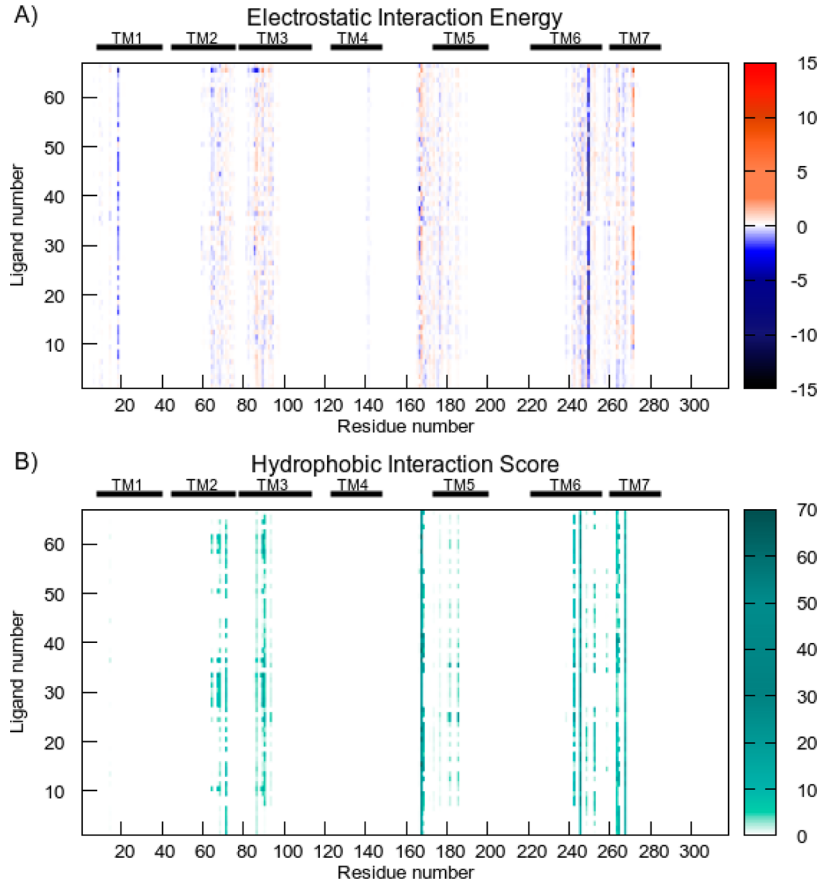

Figure 1. (A) Per residue electrostatic interaction energy map and (B) per residue hydrophobic interaction score map. The maps are calculated for a selected pose of each compound (**3**–**62**) inside the hA_3 AR binding site. Electrostatic energy values are expressed in kcal mol^{-1}, whereas hydrophobic scores are expressed in arbitrary hydrophobic units.

template. Moreover, docking simulations at the hA_{2A} AR binding site were also performed to explain the hA_{2A}/hA_3 selectivity profile.

In addition, to analyze the ligand–receptor recognition mechanism in a more quantitative fashion, we calculated the individual electrostatic and hydrophobic contributions to the interaction energy of each receptor residue involved in the binding with the ligands. The analysis of these contributions afforded "interaction energy fingerprints" (hereby indicated as IEFs), i.e., interaction energy patterns, graphically displayed either as histograms or as 3D color maps, reporting the key residues involved in the binding with the considered ligands along with a quantitative estimate of the occurring interactions. Such analysis provides some information at a glance: On one side, the identification of the key residues involved in the interactions highlights possible trends in the binding modes of the considered derivatives. On the other side, the semiquantitative analysis of the interactions allows a direct comparison of different ligands with respect to the quality of ligand–receptor contacts. Figure 1 displays the calculated electrostatic and hydrophobic contributions to the interaction energy to the hA3 AR for the energetically more favorable pose of each compound investigated. Most of the selected poses share a common interacting network with residues located in TM2, TM3, TM6, TM7, and EL2. The map of the electrostatic IEFs (Figure 1A) shows an intense band with negative potential energy (colored in blue) corresponding to Asn250 (6.55) in TM6, suggesting that this residue is responsible for the main electrostatic interactions with all the tested analogues, with a few exceptions. Asn250 (6.55) in TM6 is highly conserved among all AR subtypes and believed to play a role in ligand binding to the hA3 AR.[33,34] On the other hand, the map of the hydrophobic IEFs (Figure 1B) highlights several residues involved in hydrophobic contacts with the ligands, such as Leu68 (2.60), Val72 (2.64) in TM2, Leu90 (3.31) and Leu91 (3.32) in TM3, Phe168 and Val169 in EL2, Trp243 (6.48), Leu246 (6.51) and Ile253 (6.58) in TM6, and Ile268 (7.39) in TM7.

The same interaction patterns have also been observed for the energetically more favorable pose of the ligands at the hA_{2A} AR (Figure S1, Supporting Information): In particular, the compounds establish electrostatic interactions with Asn253 (6.55) and Glu169 (EL2) and hydrophobic contacts with, among others, Ile66 (2.64), Val84 (3.32), Phe168 (EL2), Leu249 (6.51), and Ile274 (7.39). Consistently with their lower activity at the hA_{2A} AR, the *per residue* contributions are weaker with respect to those calculated for the interactions with the hA_3 AR residues. The general trend that emerged from the above-described maps has also been confirmed by a detailed analysis of the docking poses, as reported below.

*Docking of 5-Alkylamino Derivatives (compounds **5**–**62**).* A first glance at the docking poses of the new derivatives has revealed that the compounds share at least two common hypothetical binding modes (Figure 2A,B), which differ in the orientation of the ligand in the binding cleft: In the first binding mode (hereafter indicated as BM1), the substituent at the N^5 position points away from the binding pocket (Figure 2A),

dx.doi.org/10.1021/jm300899q | J. Med. Chem. 2012, 55, 9654–9668

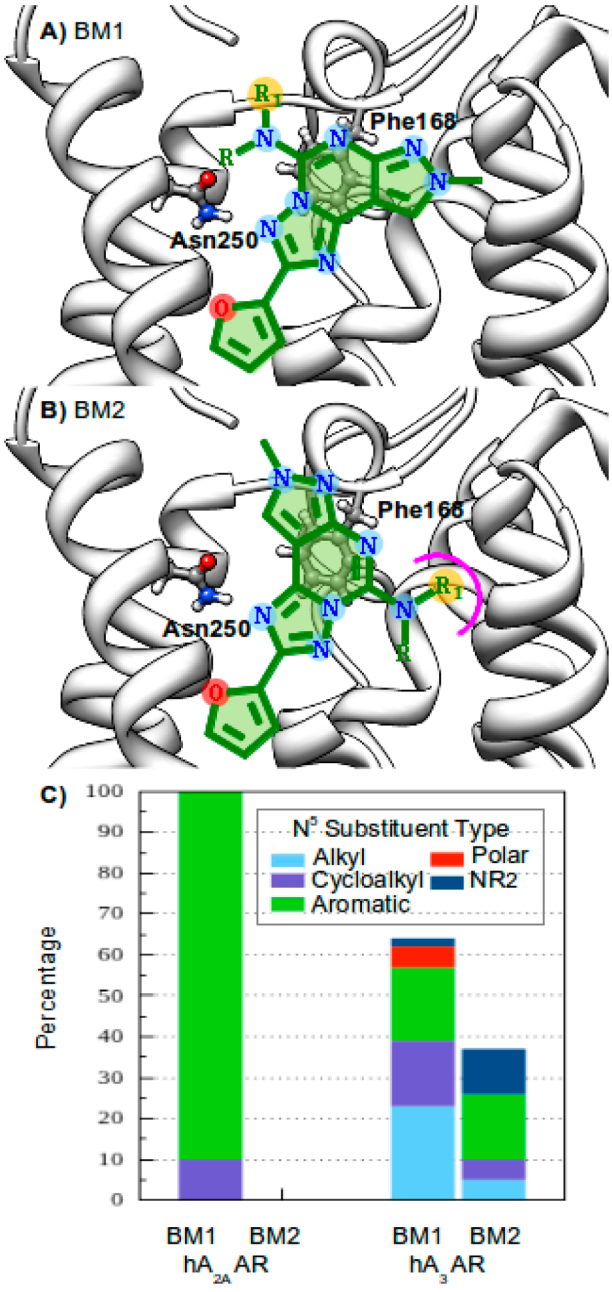

Figure 2. Schematic representation of the two binding modes BM1 (A) and BM2 (B) inside the hA_3 AR. The side chain of Asn250 (6.55) and Phe168 (EL2) are displayed in ball and stick. (C) Statistical analysis of the occurrence of the two binding modes for the ligands showing K_i < 100 nM at both hA_3 AR and hA_{2A} AR. The histograms are color-coded according to the nature of the substituent at the N^5 position.

whereas in the other binding mode (hereafter indicated as BM2) the substituent lies inside the binding cavity (Figure 2B).

The statistical analysis of the occurrence of the two binding modes (Figure 2C) performed for the compounds showing K_i < 100 nM reveals an interesting trend: None of the ligands exhibits BM2 at the hA_{2A} AR, whereas at the hA_3 AR, the latter is the preferred binding mode for the 36% of the compounds. This suggests that, while the adoption of BM2 might hamper the ligand to establish interactions with key residues at the hA_{2A} AR, it might represent an effective binding mode at the hA_3 AR. The color code of the histograms in Figure 2C highlights that the direction of the substituent at the N^5 position strongly depends on its nature and size: Compounds bearing small alkyl and cycloalkyl groups and polar chains prefer BM1, whereas the majority of the ligands bearing aromatic rings, bulky substituents as well as those with the double substitution at the N^5 atom, preferentially adopt BM2. To understand the reasons for the differences in the direction of the substituents that at the hA_3 AR reflect the above-mentioned binding modes, two reference compounds (one for each binding mode) have been selected, and their energetically more favorable docking poses along with the main interactions occurring between the ligands and the receptor are discussed herein. Figure 3A,B displays the hypothetical binding modes of **50** (K_i = 38.6 nM, Figure 2A) and **35** (K_i = 0.83 nM, Figure 2B) at the hA_3 AR as examples of compounds adopting BM1 and BM2, respectively. In both cases, the ligand recognition occurs in the upper region of the TM bundle with the PTP scaffold surrounded by TM3, TM5, TM6, and TM7, the 2-furyl ring oriented toward TM5. The key interactions are represented by one and two hydrogen bonds with Asn250 (6.55) for **50** and **35**, respectively, a $\pi-\pi$ stacking interaction between the PTP core and Phe168 (EL2), and hydrophobic contacts with, among others, Trp243 (6.48) and Leu246 (6.51). The placement of compound **35** into the binding cleft resembles that observed for the 1,2,4-triazine adenosine A_{2A} AR antagonists, that have been recently cocrystallized with the receptor.[35]

As stated above, the two BMs differ in the orientation of the substituent at the N^5 position. Figure 2C shows the hA_3 AR embedded in a lipid bilayer simulating the cellular membrane and helps in visualizing the difference: in BM1 (green arrow) the substituent at the N^5 position is directed away from the binding cleft, thus being exposed to solvent, whereas in BM2 (orange arrow) the substituent at the N^5 position points toward the binding cavity. As highlighted by the different colors of the residue side chains in Figure 2C and reported in the IEF analysis in Figure 2D, the two BMs result from the interaction of the substituent at the N^5 position with different TMs. In particular, compound **50** (BM1) establishes hydrophobic contacts mainly with residues in TM6, TM7, and EL2, the most prominent being Val169 (EL2), Trp243 (6.48), Leu246 (6.51), and Ile268 (7.39). Compound **35**, instead, interacts mainly with residues sited in TM2, TM3, and EL2, such as Leu68 (2.60), Val72 (2.64), Leu90 (3.31), Trp243 (6.48), Leu246 (6.51), and Ile268 (7.39).

The values of the interaction energies in Figure 2D also reveal that the adoption of BM2 (orange histograms) causes the ligand to establish a weaker electrostatic interaction with Asn250 (6.55) with respect to BM1 (green histograms), which however seems to be counter-balanced by stronger hydrophobic contacts with residues in TM2 and TM3. Of course, this hypothesis might be expected to be the result of a docking artifact, considering the well-documented limitations/approximations of docking methods. Very recently, we presented a novel approach obtained by the integration of molecular docking and membrane molecular dynamics simulations with the aim to merge the main advantage of docking, that is the rapid sampling of ligand poses into the binding site, with the thermodynamic accuracy of MD simulations in particular regarding the description, at the molecular level, of the stability of a GPCR–ligand complex embedded into an explicit lipid–water environment.[36] In this approach we can try to overcome some of the most crucial approximations of the conventional scoring functions such as the absence of explicit water molecules and the explorations of

dx.doi.org/10.1021/jm300899q | J. Med. Chem. 2012, 55, 9654–9668

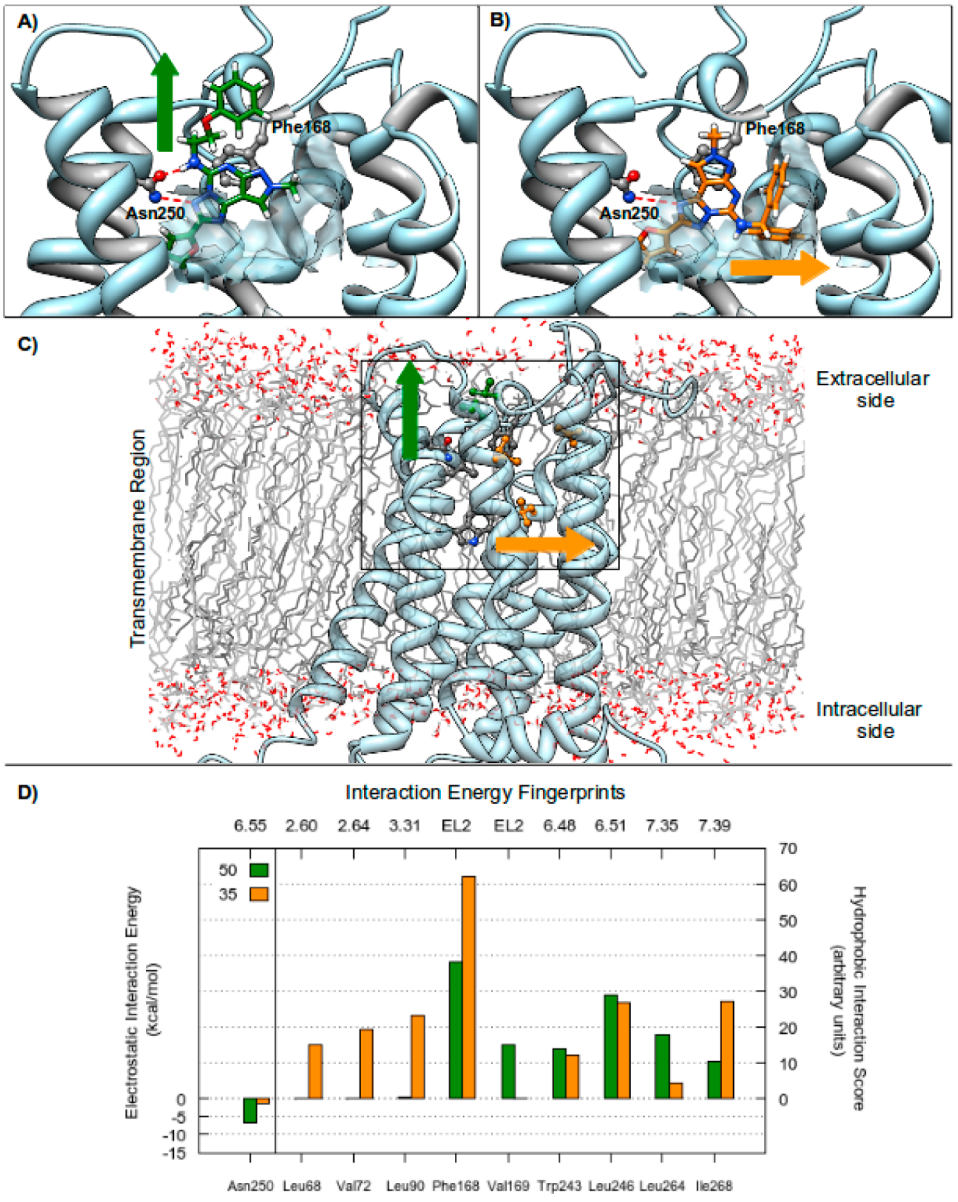

Figure 3. Hypothetical binding modes of compound **50** (A) and **35** (B) inside the hA_3 AR binding site. Poses are viewed from the membrane side facing TM6, TM7, and TM1 with the view of TM7 partially omitted to aid visualization. The side chains of Asn250 (6.55) and Phe168 (EL2) and the N^5 atom are represented in ball and stick. Hydrogen bond interactions are highlighted as dashed lines, whereas the side chains of residues interacting with the ligand through hydrophobic contacts are displayed as surfaces. An arrow indicating the directionality of the substituent at the N^5 position is shown. (C) Schematic representation of the hA_3 AR embedded in a solvated lipid bilayer simulating the cell membrane. The side chains of residues interacting through hydrophobic contacts are displayed as green and orange ball and sticks, for BM1 and BM2, respectively. Side chains of Asn250 (6.55), Phe168 (EL2), and Trp243 (6.48) are represented in gray ball and stick. Hydrogen atoms are omitted. (D) IEF analysis for compounds **50** and **35**.

receptor–ligand complex flexibility that have been recently reported to be very important in determining the binding energetics of the GPCR–ligand complex.[37] Therefore, to evaluate the reliability of the above-described BMs, we performed molecular dynamics (MD) simulations and investigated the evolution of the interactions suggested by the IEF analysis during a time lapse of 60 ns.

Molecular Dynamics. The ligand–receptor complexes of the two reference compounds **35** and **50** have been embedded in a 1-palmitoyl-2-oleoyl-*sn*-glycero-3-phosphocholine (POPC) lipid bilayer and subjected to MD simulations. The analysis of the MD trajectory and the corresponding IEFs of **50** (Figure S2A, Supporting Information) highlights that the interaction pattern that emerged from the analysis of the docking poses is conserved throughout the simulation. In particular, the interactions with Asn250 (6.55), Phe168 (EL2), Leu246 (6.51), and Leu90 (3.31) are constant during the considered time lapse. Moreover, during the simulation, the PTP core establishes strong hydrogen bond interactions with Gln167 (data not shown), which is recruited from EL2 and contributes to further stabilize the ligand–receptor interaction. These results along with the low average fluctuation of the ligand (2.28 ± 0.77 Å) supports the high degree of fitness of the selected starting conformation. The same can be asserted for **35** (Figure S2B), which shows a strong and persistent ligand–receptor interaction network with negligible ligand fluctuations (average 2.21 ± 0.59 Å). Therefore, the favorable

dx.doi.org/10.1021/jm300899q | *J. Med. Chem.* 2012, 55, 9654–9668

and hydrophobic contacts with the binding pocket delimited by TM2 and TM3 may be considered a valid rationalization of the activity of **35** at the hA_3 AR. On the whole, the above-described results have helped in defining the structure affinity profiles of the new 5-alkylamino scaffold.

The analysis of the docking poses performed through visual inspection, statistical analysis of the occurrence of the observed BMs, and IEF analyses have highlighted that the placement of the ligands into the binding cavity is mainly driven by the nature and size of the substituents at the N^5 position. In particular, compounds bearing small alkyl and cycloalkyl groups as well as polar chains preferentially direct the substituent away from the binding pocket by adopting BM1, whereas the inclusion of aromatic rings, bulky substituents, and double substitution at the N^5 atom (also with the inclusion of the nitrogen atom into certain heterocycles) causes the ligand to adopt a different placement with the substituent pointing toward regions of the binding site rich with residues bearing hydrophobic side chains (BM2). The latter orientation, at the hA_3 AR, allows the PTP to interact with the two key residues Asn250 (6.55) and Phe168 (EL2) and establish strong and favored interactions with residues in TM2 and TM3. Conversely, this interaction pattern has not been observed at the hA_{2A} AR, as all the active compounds exhibit BM1.

This is consistent with the putative different electrostatic potentials of the residues that surround the binding cavity in the two receptor subtypes: In fact, the hA_{2A} AR bears a charged gate (represented by the ionic couple Glu169 (EL2)-His264 (EL3)) at the binding site entrance that does not allow ligands with bulky and hydrophobic substituents to approach key residues in the binding cleft. The hA_3 AR binding site, instead, lacks this ionic gate, as Glu169 is mutated to Val169: Therefore, according to our proposed model and as emerged from MD simulations, its binding pocket can accommodate bulky substituents better than the other AR subtypes. These results therefore enforces our hypothesis that the presence of the charged gate at the binding site entrance in hA_{2A} AR might affect the ligand orientation and its placement into the binding cleft.[31]

CONCLUSIONS

We have presented a novel series of 5-alkylaminopyrazolo-[4,3-*e*]1,2,4-triazolo[1,5-*c*]pyrimidines acting as antagonists of the hA_3 AR. We have analyzed the corresponding SAR with the aim to establish the directionality of 5-substitutions inside the orthosteric binding site of the hA_3 AR. Interestingly, almost all the synthesized compounds showed affinity for the hA_3 AR from nanomolar to subnanomolar range with the most potent and selective antagonist bearing an (*S*) α-phenylethylamino moiety at the 5 position (**26**, hA_3 AR K_i = 0.3 nM). Using an in silico receptor-driven approach, we have determined the most favorable orientation of the substitutions at the 5-position of the PTP scaffold, opening the possibility for further scaffold decorations that point the N^5 position toward the extracellular environment. In particular, it can be concluded that small alkyl and cycloalkyl groups as well as polar chains might be suitable functionalizing moieties at the N^5 site for the linkage of fluorophore groups as well as other "sensoring" moieties that can be useful for the investigation of the physiological and physiopathological functions of ARs. Especially, chain-elongated alkyl groups, as long as not bulky and sterically hindered, might represent an effective choice. Moreover, in the light of the obtained results, a higher degree of selectivity toward either the hA_3 AR or the hA_{2A} AR subtype might be afforded by taking into account the different electrostatic potentials of the binding site entrance and by tailoring the physicochemical properties of the PTP scaffold accordingly to the desired target.

EXPERIMENTAL SECTION

A. Chemistry. Reactions were routinely monitored by thin-layer chromatography (TLC) on silica gel (precoated F_{254} Merck plates). Infrared spectra (IR) were measured on a Jasco FT-IT instrument. ^{1}H NMR were determined in $CDCl_3$ or DMSO-d_6 solutions with a Varian Gemini 200 spectrometer, peaks positions are given in parts per million (δ) downfield from tetramethylsilane as internal standard, and *J* values are given in hertz. Electrospray mass spectra were recorded on a ESI Bruker 4000 Esquire spectrometer (University of Trieste), and compounds were dissolved in methanol. Light petroleum ether refers to the fractions boiling at 40−60 °C. Melting points were determined on a Büchi-Tottoli instrument and are uncorrected. Flash chromatography was performed using Merck 60−200 mesh silica gel. Elemental analyses were performed by the microanalytical laboratory of Dipartimento di Chimica, University of Trieste, and were within ±0.4% of the theoretical values for C, H, and N.

*2-Furan-2-yl-8-methyl-6,8-dihydropyrazolo[4,3-e][1,2,4]triazolo-[1,5-c]pyrimidin-5-one (**64**).* Compound **63** (200 mg, 0.869 mmol) was dissolved in dry dioxane, and diphosgene was added (1.13 mmol, 0.136 mL). The mixture was heated at 70 °C for 1.5 h. The reaction was monitored by TLC (EtOAc:MeOH, 9:1), and when the starting material disappeared, the solvent was removed. Product **64** was precipitated from EtOAc and petroleum ether, obtaining an ivory powder that was used without further purification. Yield 46%; ivory solid (EtOAc/petroleum ether) mp >300 °C; ^{1}H NMR (DMSO-d_6) δ: 3.96 (3H, s), 6.71 (1H, dd, *J* = 2, *J* = 4), 7.18 (1H, d, *J* = 4), 7.93 (1H, d, *J* = 2), 8.58 (1H, s). IR (Nujol) cm^{-1}: 3345−3270, 1695, 1620, 1510, 1430. ES-MS (methanol): 279.00 (M + 23). Anal. ($C_{11}H_8N_6O_2$) C, H, N.

*5-Chloro-2-furan-2-yl-8-methyl-8H-pyrazolo[4,3-e][1,2,4]-triazolo[1,5-c]pyrimidine (**65**).* Compound **64** (100 mg, 0.390 mmol) was dissolved in phosphoryl chloride (21.46 mmol, 2 mL), and phosphorus pentachloride (0.117 mmol, 24 mg) and pyridine (0.975 mmol, 0.079 mL) were added. The mixture was refluxed for 24 h, the solvent was removed under reduced pressure, and the residue was dissolved in chloroform and washed with water and brine (1:1). The organic layer was dried and concentrated, and the residue purified through flash chromatography using EtOAc:MeOH 9.5:0.5 to afford the desired compound **65**. Yield 34%; white solid (EtOAc/petroleum ether) mp 285 °C; ^{1}H NMR (DMSO-d_6) δ: 4.12 (3H, s), 6.73 (1H, dd, *J* = 2, *J* = 4), 7.22 (1H, d, *J* = 4), 7. 95 (1H, d, *J* = 2), 8.61 (1H, s). IR (Nujol) cm^{-1}: 1625, 1500, 1415. ES-MS (methanol): 297.00 (M + 23). Anal. ($C_{11}H_7N_6OCl$) C, H, N.

*General Procedure for the Synthesis of the 5-Alkoxy-2-furan-2-yl-8-methyl-8H-pyrazolo[4,3-e][1,2,4]triazolo[1,5-c]pyrimidine (**3**, **4**).* To 5 mL of ethanol or methanol was added 8.3 mg (0.364 mmol) of sodium. When all the sodium was consumed, 100 mg of 5-chloro derivative **65** was added to the solution (0.364 mmol). Reaction was refluxed 2 h and monitored through TLC (EtOAc). Then, the solvent was removed under pressure and the residue purified by flash chromatography (EtOAc:petroleum ether, 9:1), affording the desired compounds.

*2-(Furan-2-yl)-5-methoxy-8-methyl-8H-pyrazolo[4,3-e][1,2,4]-triazolo[1,5-c]pyrimidine (**3**).* Yield 75%; pale brown solid (EtOAc/petroleum ether) mp 250 °C; ^{1}H NMR ($CDCl_3$) δ: 4.17 (3H, s), 4.36 (3H, s), 6.58 (1H, dd, *J* = 2, *J* = 4), 7.26 (1H, d, *J* = 4), 7.62 (1H, d, *J* = 2), 8.18 (1H, s). IR (Nujol) cm^{-1}: 1630, 1510, 1420. Anal. ($C_{12}H_{10}N_6O_2$) C, H, N.

*5-Ethoxy-2-(furan-2-yl)-8-methyl-8H-pyrazolo[4,3-e][1,2,4]-triazolo[1,5-c]pyrimidine (**4**).* Yield 73%; pale yellow solid (EtOAc/petroleum ether) mp 223 °C; ^{1}H NMR ($CDCl_3$) δ: 1.43 (3H, t, *J* = 7), 4.16 (3H, s), 4.40 (2H, q, *J* = 7), 6.59 (1H, dd, *J* = 2, *J* = 4), 7.24 (1H, d, *J* = 4), 7. 62 (1H, d, *J* = 2), 8.16 (1H, s). IR (Nujol) cm^{-1}: 1635, 1515, 1420. Anal. ($C_{13}H_{12}N_6O_2$) C, H, N.

*General Procedure for the Synthesis of the 5-Amino-Substituted 2-Furan-2-yl-8-methyl-8H-pyrazolo[4,3-e][1,2,4]triazolo[1,5-c]-pyrimidine (**5**−**62**).* 5-Chloro derivative **65** (100 mg, 0.364 mmol) was

dx.doi.org/10.1021/jm300899q | J. Med. Chem. 2012, 55, 9654−9668

dissolved in 5 mL of ethanol, triethylamine (TEA, 0.364 mmol, 51 μL) and the appropriate amine (1.092 mmol) were added, and the mixture was heated at 110 °C in a sealed tube for 2 h. The reaction was monitored through TLC (EtOAc:MeOH, 9:1). Then, the solvent was removed under reduced pressure and the residue purified by flash chromatography (EtOAc:MeOH 9.5:0.5) affording the desired compound.

(2-Furan-2-yl-8-methyl-8H-pyrazolo[4,3-e][1,2,4]triazolo[1,5-c]-pyrimidin-5-yl)methylamine (**5**). Yield 75%; pale yellow solid (EtOAc/petroleum ether) mp 285 °C; ^{1}H NMR ($CDCl_3$) δ: 3.24 (3H, d, J = 5), 4.11 (3H, s), 6.23 (1H, bs), 6.60 (1H, dd, J = 2, J = 4), 7.18 (1H, d, J = 4), 7.61 (1H, d, J = 2), 8.07 (1H, s). IR (Nujol) cm^{-1}: 3350−3170, 1615, 1520, 1410. Anal. ($C_{12}H_{11}N_7O$) C, H, N.

Ethyl(2-furan-2-yl-8-methyl-8H-pyrazolo[4,3-e][1,2,4]triazolo-[1,5-c]pyrimidin-5-yl)amine (**6**). Yield 83%; pale yellow solid (EtOAc/petroleum ether) mp 256 °C; ^{1}H NMR ($CDCl_3$) δ: 1.38 (3H, t, J = 7), 3.68−3.78 (2H, m), 4.10 (3H, s), 6.21 (1H, bs), 6.58 (1H, dd, J = 2, J = 4), 7.18 (1H, d, J = 4), 7.62 (1H, d, J = 2), 8.07 (1H, s). IR (Nujol) cm^{-1}: 3330.3180, 1630, 1505, 1420. ES-MS (methanol) m/z: 284.10 (M + 1),306.10 (M + 23). Anal. ($C_{13}H_{13}N_7O$) C, H, N.

(2-Furan-2-yl-8-methyl-8H-pyrazolo[4,3-e][1,2,4]triazolo[1,5-c]-pyrimidin-5-yl)isopropylamine (**7**). Yield 78%; pale yellow solid (EtOAc/petroleum ether) mp 214 °C; ^{1}H NMR ($CDCl_3$) δ: 1.40 (6H, d, J = 6), 4.11 (3H, s), 4.46−4.47 (1H, m), 6.08 (1H, d, J = 8), 6.60 (1H, dd, J = 2, J = 4), 7.22 (1H, d, J = 4), 7.63 (1H, d, J = 2), 8.10 (1H, s). IR (Nujol) cm^{-1}: 3340−3150, 1625, 1510, 1415. Anal. ($C_{14}H_{15}N_7O$) C, H, N.

(R,S)-(+,−)-sec-Butyl-(2-furan-2-yl-8-methyl-8H-pyrazolo[4,3-e]-[1,2,4]triazolo[1,5-c]pyrimidin-5-yl)amine (**8**). Yield 77%; white solid (EtOAc/petroleum ether) mp 190 °C; ^{1}H NMR ($CDCl_3$) δ: 1.01 (3H, t, J = 7), 1.35 (3H, t, J = 7), 1.60−1.83 (2H, m), 4.10 (3H, s), 4.25−4.45 (1H, m), 6.05 (1H, d, J = 8), 6.59 (1H, dd, J = 2, J = 4), 7.20 (1H, d, J = 4), 7.62 (1H, d, J = 2), 8.08 (1H, s). IR (Nujol) cm^{-1}: 3335−3165, 1615, 1510, 1405. Anal. ($C_{15}H_{17}N_7O$) C, H, N.

(S)-(+)-sec-Butyl-(2-furan-2-yl-8-methyl-8H-pyrazolo[4,3-e]-[1,2,4]triazolo[1,5-c]pyrimidin-5-yl)amine (**9**). Yield 65%; old pink solid (EtOAc/petroleum ether) mp 162 °C; ^{1}H NMR ($CDCl_3$) δ: 1.01 (3H, t, J = 7), 1.35 (3H, t, J = 7), 1.59−1.85 (2H, m), 4.11 (3H, s), 4.27−4.45 (1H, m), 6.07 (1H, d, J = 8), 6.60 (1H, dd, J = 2, J = 4), 7.30 (1H, d, J = 4), 7.64 (1H, d, J = 2), 8.19 (1H, s). IR (Nujol) cm^{-1}: 3345−3160, 1625, 1520, 1405. Anal. ($C_{15}H_{17}N_7O$) C, H, N.

(R)-(−)-sec-Butyl-(2-furan-2-yl-8-methyl-8H-pyrazolo[4,3-e]-[1,2,4]triazolo[1,5-c]pyrimidin-5-yl)amine (**10**). Yield 82%; old pink solid (EtOAc/petroleum ether) mp 180 °C; ^{1}H NMR ($CDCl_3$) δ: 1.01 (3H, t, J = 7), 1.35 (3H, t, J = 7), 1.59−1.83 (2H, m), 4.10 (3H, s), 4.23−4.45 (1H, m), 6.07 (1H, d, J = 8), 6.60 (1H, dd, J = 2, J = 4), 7.28 (1H, d, J = 4), 7.64 (1H, d, J = 2), 8.17 (1H, s). IR (Nujol) cm^{-1}: 3335−3150, 1630, 1500, 1415. Anal. ($C_{15}H_{17}N_7O$) C, H, N.

(2-Furan-2-yl-8-methyl-8H-pyrazolo[4,3-e][1,2,4]triazolo[1,5-c]-pyrimidin-5-yl)pentylamine (**11**). Yield 74%; pale yellow solid (EtOAc/petroleum ether) mp 157 °C; ^{1}H NMR ($CDCl_3$) δ: 1.01 (3H, t, J = 7), 1.33−1.52 (4H, m), 1.67−1.83 (2H, m), 3.67 (2H, q, J = 7), 4.10 (3H, s), 6.26 (1H, bs), 6.59 (1H, dd, J = 2, J = 4), 7.22 (1H, d, J = 4), 7.62 (1H, d, J = 2), 8.09 (1H, s). IR (Nujol) cm^{-1}: 3340−3160, 1615, 1520, 1415. Anal. ($C_{16}H_{19}N_7O$) C, H, N.

(2-Furan-2-yl-8-methyl-8H-pyrazolo[4,3-e][1,2,4]triazolo[1,5-c]-pyrimidin-5-yl)-(1-methylhexyl)amine (**12**). Yield 88%; yellow solid (EtOAc/petroleum ether) mp 150 °C; ^{1}H NMR ($CDCl_3$) δ: 0.87 (3H, t, J = 7), 1.19−1.73 (11H, m), 4.10 (3H, s), 4.33−4.56 (1H, m), 6.04 (1H, d, J = 8), 6.59 (1H, dd, J = 2, J = 4), 7.20 (1H, d, J = 4), 7.62 (1H, d, J = 2), 8.07 (1H, s). IR (Nujol) cm^{-1}: 3350−3150, 1625, 1500, 1420. Anal. ($C_{18}H_{23}N_7O$) C, H, N.

(2-Furan-2-yl-8-methyl-8H-pyrazolo[4,3-e][1,2,4]triazolo[1,5-c]-pyrimidin-5-yl)-(1-methylheptyl)amine (**13**). Yield 84%; yellow solid (EtOAc/petroleum ether) mp 149 °C; ^{1}H NMR ($CDCl_3$) δ: 0.85 (3H, t, J = 7), 1.13−1.55 (11H, m), 1.57−1.73 (2H, m), 4.09 (3H, s), 4.33−4.55 (1H, m), 5.81 (1H, d, J = 9), 6.60 (1H, dd, J = 2, J = 4), 7.22 (1H, d, J = 4), 7.63 (1H, d, J = 2), 8.09 (1H, s). IR (Nujol) cm^{-1}: 3345−3165, 1615, 1510, 1400. Anal. ($C_{19}H_{25}N_7O$) C, H, N.

(2-Ethylhexyl)(2-furan-2-yl-8-methyl-8H-pyrazolo[4,3-e][1,2,4]-triazolo[1,5-c]pyrimidin-5-yl)amine (**14**). Yield 72%; pale yellow solid (EtOAc/petroleum ether) mp 114 °C; ^{1}H NMR ($CDCl_3$) δ: 0.89−0.98 (6H, m), 1.27−1.53 (8H, m), 1.68−1.81 (1H, m), 3.62 (2H, t, J = 6), 4.10 (3H, s), 6.22 (1H, bs), 6.58 (1H, dd, J = 2, J = 4), 7.23 (1H, d, J = 4), 7.63 (1H, d, J = 2), 8.10 (1H, s). IR (Nujol) cm^{-1}: 3335−3150, 1645, 1520, 1415. Anal. ($C_{19}H_{25}N_7O$) C, H, N.

(2-Furan-2-yl-8-methyl-8H-pyrazolo[4,3-e][1,2,4]triazolo[1,5-c]-pyrimidin-5-yl)-(1,1,3,3-tetramethylbutyl)amine (**15**). Yield 81%; pale yellow solid (EtOAc/petroleum ether) mp 176 °C; ^{1}H NMR ($CDCl_3$) δ: 1.03 (9H, s), 1.68 (6H, s), 2.04 (2H, s), 4.10 (3H, s), 6.29 (1H, bs), 6.58 (1H, dd, J = 2, J = 4), 7.22 (1H, d, J = 4), 7.62 (1H, d, J = 2), 8.10 (1H, s). IR (Nujol) cm^{-1}: 3330−3140, 1635, 1520, 1410. Anal. ($C_{19}H_{25}N_7O$) C, H, N.

Cyclopropyl(2-furan-2-yl-8-methyl-8H-pyrazolo[4,3-e][1,2,4]-triazolo[1,5-c]pyrimidin-5-yl)amine (**16**). Yield 88%; yellow solid (EtOAc/petroleum ether) mp 280 °C; ^{1}H NMR ($CDCl_3$) δ: 0.75−0.82 (2H, m), 0.95−1.00 (2H, m), 2.95−3.15 (1H, m), 4.12 (3H, s), 6.43 (1H, bs), 6.60 (1H, dd, J = 2, J = 4), 7.20 (1H, d, J = 4), 7.62 (1H, d, J = 2), 8.09 (1H, s). IR (Nujol) cm^{-1}: 3340−3160, 1620, 1505, 1425. Anal. ($C_{14}H_{13}N_7O$) C, H, N.

Cyclobutyl(2-furan-2-yl-8-methyl-8H-pyrazolo[4,3-e][1,2,4]-triazolo[1,5-c]pyrimidin-5-yl)amine (**17**). Yield 80%; light brown solid (EtOAc/petroleum ether) mp 250 °C; ^{1}H NMR ($CDCl_3$) δ: 1.73−1.91 (2H, m), 1.98−2.21 (2H, m), 2.45−2.63 (2H, m), 4.10 (3H, s), 4.71−4.83 (1H, m), 6.37 (1H, d, J = 7), 6.60 (1H, dd, J = 2, J = 4), 7.21 (1H, d, J = 4), 7.63 (1H, d, J = 2), 8.06 (1H, s). IR (Nujol) cm^{-1}: 3350−3170, 1620, 1510, 1425. Anal. ($C_{15}H_{15}N_7O$) C, H, N.

Cyclopentyl(2-furan-2-yl-8-methyl-8H-pyrazolo[4,3-e][1,2,4]-triazolo[1,5-c]pyrimidin-5-yl)amine (**18**). Yield 76%; pale brown solid (EtOAc/petroleum ether) mp 226 °C; ^{1}H NMR ($CDCl_3$) δ: 1.59−2.00 (6H, m), 2.14−2.34 (2H, m), 4.10 (3H, s), 4.54−4.62 (1H, m), 6.18 (1H, d, J = 7), 6.59 (1H, dd, J = 2, J = 4), 7.20 (1H, d, J = 4), 7.62 (1H, d, J = 2), 8.06 (1H, s). IR (Nujol) cm^{-1}: 3345−3160, 1640, 1530, 1410. Anal. ($C_{16}H_{17}N_7O$) C, H, N.

Cyclohexyl(2-furan-2-yl-8-methyl-8H-pyrazolo[4,3-e][1,2,4]-triazolo[1,5-c]pyrimidin-5-yl)amine (**19**). Yield 63%; brown solid (EtOAc/petroleum ether) mp 188 °C; ^{1}H NMR ($CDCl_3$) δ: 1.25−1.92 (8H, m), 2.15−2.24 (2H, m), 4.09−4.19 (4H, m), 6.10 (1H, bs), 6.58 (1H, dd, J = 2, J = 4), 7.20 (1H, d, J = 4), 7.62 (1H, d, J = 2), 8.06 (1H, s). IR (Nujol) cm^{-1}: 3340−3150, 1625, 1510, 1415. Anal. ($C_{17}H_{19}N_7O$) C, H, N.

Cycloheptyl(2-furan-2-yl-8-methyl-8H-pyrazolo[4,3-e][1,2,4]-triazolo[1,5-c]pyrimidin-5-yl)amine (**20**). Yield 76%; orange solid (EtOAc/petroleum ether) mp 130 °C; ^{1}H NMR ($CDCl_3$) δ: 1.50−1.89 (10H, m), 2.15−2.31 (2H, m), 4.10 (3H, s), 4.32−4.45 (1H, m), 6.19 (1H, d, J = 8), 6.60 (1H, dd, J = 2, J = 4), 7.20 (1H, d, J = 4), 7.63 (1H, d, J = 2), 8.07 (1H, s). IR (Nujol) cm^{-1}: 3335−3140, 1620, 1530, 1435. Anal. ($C_{18}H_{21}N_7O$) C, H, N.

Cyclooctyl(2-furan-2-yl-8-methyl-8H-pyrazolo[4,3-e][1,2,4]-triazolo[1,5-c]pyrimidin-5-yl)amine (**21**). Yield 78%; brown solid (EtOAc/petroleum ether) mp 149 °C; ^{1}H NMR ($CDCl_3$) δ: 1.61−2.15 (14H, m), 4.10 (3H, s), 4.35−4.53 (1H, m), 6.19 (1H, d, J = 8), 6.60 (1H, dd, J = 2, J = 4), 7.21 (1H, d, J = 4), 7.63 (1H, d, J = 2), 8.07 (1H, s). IR (Nujol) cm^{-1}: 3355−3160, 1635, 1505, 1425. Anal. ($C_{19}H_{23}N_7O$) C, H, N.

Cyclohexylmethyl(2-furan-2-yl-8-methyl-8H-pyrazolo[4,3-e]-[1,2,4]triazolo[1,5-c]pyrimidin-5-yl)amine (**22**). Yield 74%; brown solid (EtOAc/petroleum ether) mp 169 °C; ^{1}H NMR ($CDCl_3$) δ: 0.83−1.39 (4H, m), 1.55−1.93 (6H, m), 2.76 (1H, d, J = 7), 3.53 (2H, t, J = 7), 4.10 (3H, s), 6.33 (1H, bs), 6.60 (1H, dd, J = 2, J = 4), 7.21 (1H, d, J = 4), 7.63 (1H, d, J = 2), 8.07 (1H, s). IR (Nujol) cm^{-1}: 3355−3150, 1625, 1510, 1430. Anal. ($C_{18}H_{21}N_7O$) C, H, N.

Adamantan-1-yl(2-furan-2-yl-8-methyl-8H-pyrazolo[4,3-e]-[1,2,4]triazolo[1,5-c]pyrimidin-5-yl)amine (**23**). Yield 75%; pale yellow solid (EtOAc/petroleum ether) mp 282 °C; ^{1}H NMR ($CDCl_3$) δ: 1.67−1.83 (6H, m), 2.17 (3H, s), 2.32 (6H, s), 4.10 (3H, s), 6.14 (1H, bs), 6.60 (1H, dd, J = 4, J = 2), 7.32 (1H, d, J = 4), 7.63 (1H, d, J = 2), 8.13 (1H, s). IR (Nujol) cm^{-1}: 3345−3170, 1635, 1520, 1405. Anal. ($C_{21}H_{23}N_7O$) C, H, N.

Adamantan-2-yl(2-furan-2-yl-8-methyl-8H-pyrazolo[4,3-e]-[1,2,4]triazolo[1,5-c]pyrimidin-5-yl)amine (**24**). Yield 83%; pale yellow solid (EtOAc/petroleum ether) mp 286 °C; ^{1}H NMR ($CDCl_3$)

dx.doi.org/10.1021/jm300899q | J. Med. Chem. 2012, 55, 9654−9668

δ: 1.68−2.04 (12H, m), 2.24 (2H, s), 4.09 (3H, s), 4.44 (1H, bs), 6.53−6.58 (2H, m), 7.23 (1H, d, J = 4), 7.63 (1H, d, J = 2), 8.09 (1H, s). IR (Nujol) cm^{-1}: 3330−3140, 1640, 1520, 1405. Anal. ($C_{21}H_{23}N_7O$) C, H, N.

*Benzyl(2-furan-2-yl-8-methyl-8H-pyrazolo[4,3-e][1,2,4]triazolo-[1,5-c]pyrimidin-5-yl)amine (**25**).* Yield 87%; yellow solid (EtOAc/petroleum ether) mp 188 °C; ^1H NMR ($CDCl_3$) δ: 4.12 (3H, s), 4.87 (2H, d, J = 5), 5.56−5.62 (2H, m), 7.17−7.46 (6H, m), 7.69 (1H, d, J = 2), 8.09 (1H, s). IR (Nujol) cm^{-1}: 3350−3160, 1630, 1515, 1425. Anal. ($C_{18}H_{15}N_7O$) C, H, N.

*(S)-(2-Furan-2-yl-8-methyl-8H-pyrazolo[4,3-e][1,2,4]triazolo[1,5-c]pyrimidin-5-yl)-(1-phenylethyl)amine (**26**).* Yield 84%; pale yellow solid (EtOAc/petroleum ether) mp 189 °C; ^1H NMR ($CDCl_3$) δ: 1.72 (3H, d, J = 7), 4.09 (3H, s), 5.49−5.63 (1H, m), 6.48 (1H, bs), 6.58 (1H, dd, J = 2, J = 4), 7.19−7.39 (4H, m), 7.50 (2H, d, J = 7), 7.61 (1H, d, J = 2), 8.06 (1H, s). IR (Nujol) cm^{-1}: 3350−3170, 1640, 1510, 1425. Anal. ($C_{19}H_{17}N_7O$) C, H, N.

*(R)-(2-Furan-2-yl-8-methyl-8H-pyrazolo[4,3-e][1,2,4]triazolo[1,5-c]pyrimidin-5-yl)(1-phenylethyl)amine (**27**).* Yield 92%; yellow solid (EtOAc/petroleum ether) mp 69 °C; ^1H NMR ($CDCl_3$) δ: 1.72 (3H, d, J = 7), 4.09 (3H, s), 5.47−5.62 (1H, m), 6.48−6.63 (2H, m), 7.20−7.51 (6H, m), 7.61 (1H, d, J = 2), 8.06 (1H, s). IR (Nujol) cm^{-1}: 3350−3130, 1635, 1525, 1400. Anal. ($C_{19}H_{17}N_7O$) C, H, N.

*(2-Furan-2-yl-8-methyl-8H-pyrazolo[4,3-e][1,2,4]triazolo[1,5-c]-pyrimidin-5-yl)(4-methylbenzyl)amine (**28**).* Yield 79%; pale brown solid (EtOAc/petroleum ether) mp 160 °C; ^1H NMR ($CDCl_3$) δ: 2.45 (3H, s), 4.12 (3H, s), 5.82 (2H, d, J = 7), 6.60−6.68 (2H, m), 7.03−7.48 (5H, m), 7.70 (1H, d, J = 2), 8.19 (1H, s). IR (Nujol) cm^{-1}: 3340−3170, 1645, 1525, 1405. Anal. ($C_{19}H_{17}N_7O$) C, H, N.

*(2-Furan-2-yl-8-methyl-8H-pyrazolo[4,3-e][1,2,4]triazolo[1,5-c]-pyrimidin-5-yl)(4-methoxybenzyl)amine (**29**).* Yield 82%; pale orange solid (EtOAc/petroleum ether) mp 175 °C; ^1H NMR ($CDCl_3$) δ: 3.80 (3H, s), 4.12 (3H, s), 4.79 (2H, d, J = 5), 6.50 (1H, bs), 6.58 (1H, dd, J = 4, J = 2), 6.89 (2H, d, J = 8), 7.23 (1H, d, J = 4), 7.39 (2H, d, J = 8), 7.61 (1H, d, J = 2), 8.16 (1H, s). IR (Nujol) cm^{-1}: 3345−3150, 1625, 1535, 1415. Anal. ($C_{19}H_{17}N_7O_2$) C, H, N.

*(4-Chlorobenzyl)-(2-furan-2-yl-8-methyl-8H-pyrazolo[4,3-e]-[1,2,4]triazolo[1,5-c]pyrimidin-5-yl)amine (**30**).* Yield 79%; pale yellow solid (EtOAc/petroleum ether) mp 212 °C; ^1H NMR ($CDCl_3$) δ: 4.12 (3H, s), 4.84 (2H, d, J = 6), 6.55−6.63 (2H, m), 7.21−7.43 (5H, m), 7.61 (1H, d, J = 2), 8.12 (1H, s). IR (Nujol) cm^{-1}: 3340−3130, 1625, 1530, 1420. Anal. ($C_{18}H_{14}N_7OCl$) C, H, N.

*(4-Fluorobenzyl)(2-furan-2-yl-8-methyl-8H-pyrazolo[4,3-e]-[1,2,4]triazolo[1,5-c]pyrimidin-5-yl)amine (**31**).* Yield 84%; pale yellow solid (EtOAc/petroleum ether) mp 186 °C; ^1H NMR ($CDCl_3$) δ: 4.12 (3H, s), 4.94 (2H, d, J = 6), 6.57−6.59 (2H, m), 6.99−7.08 (2H, m), 7.22 (1H, d, J = 4), 7.41−7.47 (2H, m), 7.61 (1H, d, J = 2), 8.13 (1H, s). IR (Nujol) cm^{-1}: 3345−3150, 1630, 1515, 1425. Anal. ($C_{18}H_{14}N_7OF$) C, H, N.

*(2-Furan-2-yl-8-methyl-8H-pyrazolo[4,3-e][1,2,4]triazolo[1,5-c]-pyrimidin-5-yl)(4-trifluoromethylbenzyl)amine (**32**).* Yield 78%; pale yellow solid (EtOAc/petroleum ether) mp 172 °C; ^1H NMR ($CDCl_3$) δ: 4.12 (3H, s), 4.94 (2H, d, J = 6), 6.58 (1H, dd, J = 2, J = 4), 6.67 (1H, bs), 7.21 (1H, d, J = 4), 7.59 (5H, m), 8.12 (1H, s). IR (Nujol) cm^{-1}: 3350−3170, 1650, 1535, 1415. Anal. ($C_{19}H_{14}N_7OF_3$) C, H, N.

*(3,4-Dimethoxybenzyl)(2-furan-2-yl-8-methyl-8H-pyrazolo[4,3-e][1,2,4]triazolo[1,5-c]pyrimidin-5-yl)amine (**33**).* Yield 74%; yellow solid (EtOAc/petroleum ether) mp 109 °C; ^1H NMR ($CDCl_3$) δ: 3.88 (6H, s), 4.12 (3H, s), 4.80 (2H, d, J = 5), 6.45−6.62 (2H, m), 6.83 (1H, d, J = 7), 6.93−7.05 (2H, m), 7.19 (1H, d, J = 4), 7.60 (1H, d, J = 2), 8.10 (1H, s). IR (Nujol) cm^{-1}: 3340−3145, 1625, 1525, 1415. Anal. ($C_{20}H_{19}N_7O_3$) C, H, N.

*Biphenyl-4-ylmethyl(2-furan-2-yl-8-methyl-8H-pyrazolo[4,3-e]-[1,2,4]triazolo[1,5-c]pyrimidin-5-yl)amine (**34**).* Yield 82%; yellow solid (EtOAc/petroleum ether) mp 240 °C; ^1H NMR ($CDCl_3$) δ: 4.13 (3H, s), 4.92 (2H, d, J = 6), 6.57−6.59 (2H, m), 7.19−7.60 (11H, m), 8.11 (1H, s). IR (Nujol) cm^{-1}: 3355−3180, 1650, 1535, 1405. Anal. ($C_{24}H_{19}N_7O$) C, H, N.

*Benzhydryl(2-furan-2-yl-8-methyl-8H-pyrazolo[4,3-e][1,2,4]-triazolo[1,5-c]pyrimidin-5-yl)amine (**35**).* Yield 64%; pale yellow solid (EtOAc/petroleum ether) mp 205 °C; ^1H NMR ($CDCl_3$) δ: 4.10 (3H, s), 6.61 (1H, dd, J = 2, J = 4), 6.74 (1H, d, J = 8), 6.86 (1H, d, J = 8), 7.31−7.38 (11H, m), 7.64 (1H, d, J = 2), 8.22 (1H, s). IR (Nujol) cm^{-1}: 3350−3160, 1655, 1540, 1435. Anal. ($C_{24}H_{19}N_7O$) C, H, N.

*(2-Furan-2-yl-8-methyl-8H-pyrazolo[4,3-e][1,2,4]triazolo[1,5-c]-pyrimidin-5-yl)-2-phenethylamine (**36**).* Yield 76%; pale brown solid (EtOAc/petroleum ether) mp 120 °C; ^1H NMR ($CDCl_3$) δ: 3.08 (2H, t, J = 7), 3.89−3.96 (2H, m), 4.11 (3H, s), 5.34 (1H, bs), 6.58 (1H, dd, J = 2, J = 4), 7.16−7.37 (6H, m), 7.59 (1H, d, J = 2), 8.09 (1H, s). IR (Nujol) cm^{-1}: 3330−3155, 1620, 1525, 1405. Anal. ($C_{19}H_{17}N_7O$) C, H, N.

*[2-(3,4-Dimethoxyphenyl)ethyl](2-furan-2-yl-8-methyl-8H-pyrazolo[4,3-e][1,2,4]triazolo[1,5-c]pyrimidin-5-yl)amine (**37**).* Yield 89%; pale brown solid (EtOAc/petroleum ether) mp 165 °C; ^1H NMR ($CDCl_3$) δ: 3.01 (2H, t, J = 7), 3.87−3.97 (8H, m), 4.12 (3H, s), 6.35 (1H, bs), 6.59 (1H, dd, J = 2, J = 4), 6.81 (3H, m), 7.18 (1H, d, J = 4), 7.61 (1H, d, J = 2), 8.09 (1H, s). IR (Nujol) cm^{-1}: 3340−3165, 1620, 1505, 1420. Anal. ($C_{21}H_{21}N_7O_3$) C, H, N.

*(2-Furan-2-yl-8-methyl-8H-pyrazolo[4,3-e][1,2,4]triazolo[1,5-c]-pyrimidin-5-yl)-(1-methyl-3-phenylpropyl)amine (**38**).* Yield 71%; pale yellow solid (EtOAc/petroleum ether) mp 177 °C; ^1H NMR ($CDCl_3$) δ: 1.40 (3H, d, J = 7), 1.99−2.09 (2H, m), 2.78 (2H, t, J = 8), 4.11 (3H, s), 4.51 (1H, m), 6.08 (1H, d, J = 8), 6.60 (1H, dd, J = 2, J = 4), 7.14−7.21 (6H, m), 7.63 (1H, d, J = 2), 8.08 (1H, s). IR (Nujol) cm^{-1}: 3350−3165, 1630, 1520, 1415. Anal. ($C_{21}H_{21}N_7O$) C, H, N.

*(2-Furan-2-yl-8-methyl-8H-pyrazolo[4,3-e][1,2,4]triazolo[1,5-c]-pyrimidin-5-yl)-[2-(1H-indol-3-yl)ethyl]amine (**39**).* Yield 67%; pale brown solid (EtOAc/petroleum ether) mp 160 °C; ^1H NMR ($CDCl_3$) δ: 3.25 (2H, t, J = 7), 4.00−4.14 (5H, m), 6.54 (1H, bs), 6.60 (1H, dd, J = 2, J = 4), 6.93−7.30 (3H, m), 7.39 (2H, d, J = 6), 7.50−7.68 (2H, m), 8.11 (1H, bs), 8.33 (1H, s). IR (Nujol) cm^{-1}: 3370−3130, 1645, 1530, 1460. Anal. ($C_{21}H_{18}N_8O$) C, H, N.

*2-(2-Furan-2-yl-8-methyl-8H-pyrazolo[4,3-e][1,2,4]triazolo[1,5-c]pyrimidin-5-ylamino)ethanol (**40**).* Yield 67%; yellow solid (EtOAc/petroleum ether) mp 188 °C ^1H NMR ($CDCl_3$) δ: 3.88−4.06 (4H, m), 4.11 (3H, s), 6.62 (1H, dd, J = 2, J = 4), 7.30 (1H, d, J = 4), 7.65 (1H, d, J = 2), 8.18 (1H, s). ES-MS (methanol): 300.1 (M + 1), 322.1 (M + 23). IR (Nujol) cm^{-1}: 3550−3130, 1620, 1525, 1405. Anal. ($C_{13}H_{13}N_7O_2$) C, H, N.

*3-(2-Furan-2-yl-8-methyl-8H-pyrazolo[4,3-e][1,2,4]triazolo[1,5-c]pyrimidin-5-ylamino)propan-1-ol (**41**).* Yield 87%; pale yellow solid (EtOAc/petroleum ether) mp 185 °C; ^1H NMR ($CDCl_3$) δ: 1.97 (2H, t, J = 6), 3.76−3.94 (4H, m), 4.13 (3H, s), 4.50 (1H, bs), 6.53 (1H, dd, J = 2, J = 4), 6.74 (1H, bs), 7.40 (1H, d, J = 4), 7.66 (1H, d, J = 2), 8.31 (1H, s). IR (Nujol) cm^{-1}: 3400−3130, 1640, 1535, 1415. Anal. ($C_{14}H_{15}N_7O_2$) C, H, N.

*1-(2-Furan-2-yl-8-methyl-8H-pyrazolo[4,3-e][1,2,4]triazolo[1,5-c]pyrimidin-5-ylamino)propan-2-ol (**42**).* Yield 73%; brown solid (EtOAc/petroleum ether) mp 215 °C; ^1H NMR ($CDCl_3$) δ: 1.32 (3H, d, J = 6), 3.44−3.61 (1H, m), 3.83−3.99 (1H, m), 4.10 (3H, s), 4.11−4.31 (1H, m), 6.60−6.64 (2H, m), 7.21 (1H, d, J = 4), 7.62 (1H, d, J = 2), 8.07 (1H, s). IR (Nujol) cm^{-1}: 3450−3110, 1650, 1505, 1430. ES-MS (methanol) *m/z*: 336.1 (M + 23). Anal. ($C_{14}H_{15}N_7O_2$) C, H, N.

*2-(2-Furan-2-yl-8-methyl-8H-pyrazolo[4,3-e][1,2,4]triazolo[1,5-c]pyrimidin-5-ylamino)butan-1-ol (**43**).* Yield 75%; yellow solid (EtOAc/petroleum ether) mp 161 °C; ^1H NMR ($CDCl_3$) δ: 1.07 (3H, t, J = 7), 1.83 (2H, m), 3.80−3.85 (1H, m), 3.96−4.08 (1H, m), 4.13 (3H, s), 4.38−4.74 (2H, m), 6.45 (1H, bs), 6.63 (1H, dd, J = 2, J = 4), 7.39 (1H, d, J = 4), 7.67 (1H, d, J = 2), 8.27 (1H, s). IR (Nujol) cm^{-1}: 3400−3130, 1625, 1540, 1430. Anal. ($C_{15}H_{17}N_7O_2$) C, H, N.

*2-(2-Furan-2-yl-8-methyl-8H-pyrazolo[4,3-e][1,2,4]triazolo[1,5-c]pyrimidin-5-ylamino)propane-1,3-diol (**44**).* Yield 61%; yellow solid (EtOAc/petroleum ether) mp 215 °C; ^1H NMR ($CDCl_3$) δ: 3.66 (4H, bs), 4.02 (3H, s), 4.17 (1H, m), 4.90 (2H, bs), 6.73 (1H, dd, J = 2, J = 4), 7.07 (1H, d, J = 8), 7.23 (1H, d, J = 4), 7.94 (1H, d, J = 2), 8.59 (1H, s). IR (Nujol) cm^{-1}: 3550−3060, 1625, 1505, 1435. Anal. ($C_{14}H_{15}N_7O_3$) C, H, N.

*4-(2-Furan-2-yl-8-methyl-8H-pyrazolo[4,3-e][1,2,4]triazolo[1,5-c]pyrimidin-5-ylamino)butan-1-ol (**45**).* Yield 78%; yellow solid (EtOAc/petroleum ether) mp 161 °C; ^1H NMR ($CDCl_3$)

dx.doi.org/10.1021/jm300899q | J. Med. Chem. 2012, 55, 9654−9668

δ: 1.74−1.99 (4H, m), 3.76 (4H, bs), 4.12 (3H, s), 6.59−6.62 (2H, m), 7.34 (1H, d, J = 4), 7.65 (1H, d, J = 2), 8.24 (1H, s). IR (Nujol) cm^{-1}: 3400−3120, 1635, 1520, 1425. Anal. ($C_{15}H_{17}N_7O_2$) C, H, N.

5-(2-Furan-2-yl-8-methyl-8H-pyrazolo[4,3-e][1,2,4]triazolo[1,5-c]pyrimidin-5-ylamino)pentan-1-ol (**46**). Yield 67%; pale brown solid (EtOAc/petroleum ether) mp 81 °C; ^{1}H NMR ($CDCl_3$) δ 1.48−1.84 (6H, m), 3.65−3.75 (4H, m), 4.10 (3H, s), 6.34 (1H, bs), 6.59 (1H, dd, J = 2, J = 4), 7.23 (1H, d, J = 4), 7.62 (1H, d, J = 2), 8.11 (1H, s). IR (Nujol) cm^{-1}: 3350−3080, 1615, 1530, 1420. Anal. ($C_{16}H_{19}N_7O_2$) C, H, N.

6-(2-Furan-2-yl-8-methyl-8H-pyrazolo[4,3-e][1,2,4]triazolo[1,5-c]pyrimidin-5-ylamino)hexan-1-ol (**47**). Yield 82%; orange solid (EtOAc/petroleum ether) mp 139 °C; ^{1}H NMR ($CDCl_3$) δ: 1.48−1.79 (8H, m), 3.63−3.75 (4H, m), 4.11 (3H, s), 6.30 (1H, bs), 6.61 (1H, dd, J = 2, J = 4), 7.30 (1H, d, J = 4), 7.64 (1H, d, J = 2), 8.14 (1H, s). IR (Nujol) cm^{-1}: 3390−3100, 1650, 1525, 1415. Anal. ($C_{17}H_{21}N_7O_2$) C, H, N.

N-(2-Furan-2-yl-8-methyl-8H-pyrazolo[4,3-e][1,2,4]triazolo[1,5-c]pyrimidin-5-yl)-O-methylhydroxylamine (**48**). Yield 54%; yellow solid (EtOAc/petroleum ether) mp 205 °C; ^{1}H NMR ($CDCl_3$) δ: 4.01−4.04 (6H, m), 6.57 (1H, dd, J = 2, J = 4), 7.20 (1H, d, J = 4), 7.60 (1H, d, J = 2), 7.90 (1H, s), 8.40 (1H, bs). IR (Nujol) cm^{-1}: 3350−3150, 1630, 1515, 1405. Anal. ($C_{12}H_{11}N_7O$) C, H, N.

(2-Furan-2-yl-8-methyl-8H-pyrazolo[4,3-e][1,2,4]triazolo[1,5-c]pyrimidin-5-yl)-(2-methoxyethyl)amine (**49**). Yield 72%; brown solid (EtOAc/petroleum ether) mp 105 °C; ^{1}H NMR ($CDCl_3$) δ: 3.32 (3H, s), 3.69−4.00 (4H, m), 4.11 (3H, s), 6.60 (2H, m), 7.24 (1H, d, J = 4), 7.63 (1H, d, J = 2), 8.11 (1H, s). IR (Nujol) cm^{-1}: 3400−3160, 1635, 1505, 1420. Anal. ($C_{14}H_{15}N_7O_2$) C, H, N.

(2-Furan-2-yl-8-methyl-8H-pyrazolo[4,3-e][1,2,4]triazolo[1,5-c]pyrimidin-5-yl)-(2-phenoxyethyl)amine (**50**). Yield 54%; brown solid (EtOAc/petroleum ether) mp 140 °C; ^{1}H NMR ($CDCl_3$) δ: 4.05−4.17 (5H, m), 4.24−4.32 (2H, m), 6.59 (1H, dd, J = 2, J = 4), 6.70 (1H, bs), 6.91−6.98 (3H, m), 7.23−7.24 (3H, m), 7.63 (1H, d, J = 2), 8.12 (1H, s). IR (Nujol) cm^{-1}: 3340−3120, 1650, 1545, 1435. Anal. ($C_{19}H_{17}N_7O_2$) C, H, N.

Dimethyl-(2-furan-2-yl-8-methyl-8H-pyrazolo[4,3-e][1,2,4]triazolo[1,5-c]pyrimidin-5-yl)amine (**51**). Yield 65%; yellow solid (EtOAc/petroleum ether) mp 171 °C; ^{1}H NMR ($CDCl_3$) δ: 3.45 (6H, s), 4.13 (3H, s), 6.59 (1H, dd, J = 2, J = 4), 7.24 (1H, d, J = 4), 7.63 (1H, d, J = 2), 8.22 (1H, s). IR (Nujol) cm^{-1}: 1630, 1515, 1425. Anal. ($C_{13}H_{13}N_7O$) C, H, N.

Butyl-(2-furan-2-yl-8-methyl-8H-pyrazolo[4,3-e][1,2,4]triazolo[1,5-c]pyrimidin-5-yl)methylamine (**52**). Yield 76%; pale yellow solid (EtOAc/petroleum ether) mp 151 °C; ^{1}H NMR ($CDCl_3$) δ: 0.97 (3H, t, J = 7), 1.36−1.46 (2H, m), 1.76−1.83 (2H, m), 3.44 (3H, s), 3.94 (2H, t, J = 7), 4.14 (3H, s), 6.63 (1H, dd, J = 2, J = 4), 7.49 (1H, d, J = 4), 7.67 (1H, d, J = 2), 8.48 (1H, s). IR (Nujol) cm^{-1}: 1625, 1535, 1415. Anal. ($C_{16}H_{19}N_7O$) C, H, N.

Diethyl-(2-furan-2-yl-8-methyl-8H-pyrazolo[4,3-e][1,2,4]triazolo[1,5-c]pyrimidin-5-yl)amine (**53**). Yield 95%; yellow solid (EtOAc/petroleum ether) mp 165 °C; ^{1}H NMR ($CDCl_3$) δ: 1.38 (6H, t, J = 7), 3.95 (4H, q, J = 7), 4.10 (3H, s), 6.58 (1H, dd, J = 2, J = 4), 7.19 (1H, d, J = 4), 7.61 (1H, d, J = 2), 8.12 (1H, s). IR (Nujol) cm^{-1}: 1620, 1530, 1405. Anal. ($C_{15}H_{17}N_7O$) C, H, N.

(2-Furan-2-yl-8-methyl-8H-pyrazolo[4,3-e][1,2,4]triazolo[1,5-c]pyrimidin-5-yl)dipentylamine (**54**). Yield 81%; pale yellow solid (EtOAc/petroleum ether) mp 106 °C; ^{1}H NMR ($CDCl_3$) δ: 0.91 (6H, t, J = 7), 1.34−1.46 (8H, m), 1.68−1.87 (4H, m), 3.87 (4H, q, J = 7), 4.10 (3H, s), 6.59 (1H, dd, J = 2, J = 4), 7.18 (1H, d, J = 4), 7.62 (1H, d, J = 2), 8.12 (1H, s). IR (Nujol) cm^{-1}: 1625, 1515, 1415. Anal. ($C_{21}H_{29}N_7O$) C, H, N.

Cyclohexyl(2-furan-2-yl-8-methyl-8H-pyrazolo[4,3-e][1,2,4]triazolo[1,5-c]pyrimidin-5-yl)methylamine (**55**). Yield 78%; pale yellow solid (EtOAc/petroleum ether) mp 178 °C; ^{1}H NMR ($CDCl_3$) δ: 1.42−1.74 (4H, m), 1.85−2.04 (6H, m), 3.28 (3H, s), 4.11 (3H, s), 4.71 (1H, t, J = 7), 6.58 (1H, dd, J = 2, J = 4), 7.19 (1H, d, J = 4), 7.62 (1H, d, J = 2), 8.12 (1H, s). IR (Nujol) cm^{-1}: 1630, 1535, 1425. Anal. ($C_{18}H_{21}N_7O$) C, H, N.

Benzyl(2-furan-2-yl-8-methyl-8H-pyrazolo[4,3-e][1,2,4]triazolo[1,5-c]pyrimidin-5-yl)methylamine (**56**). Yield 78%; pale yellow solid (EtOAc/petroleum ether) mp 145 °C; ^{1}H NMR ($CDCl_3$) δ: 3.34 (3H, s), 4.13 (3H, s), 5.22 (2H, s), 6.56 (1H, dd, J = 2, J = 4), 7.16 (1H, d, J = 4), 7.30−7.40 (5H, m), 7.59 (1H, d, J = 2), 8.17 (1H, s). IR (Nujol) cm^{-1}: 1650, 1515, 1430. Anal. ($C_{19}H_{17}N_7O$) C, H, N.

Dibenzyl(2-furan-2-yl-8-methyl-8H-pyrazolo[4,3-e][1,2,4]triazolo[1,5-c]pyrimidin-5-yl)amine (**57**). Yield 62%; white solid (EtOAc/petroleum ether) mp 108 °C; ^{1}H NMR ($CDCl_3$) δ: 4.13 (3H, s), 5.15 (4H, s), 6.54 (1H, dd, J = 2, J = 4), 7.00 (1H, d, J = 4), 7.31−7.35 (10H, m), 7.59 (1H, d, J = 2), 8.17 (1H, s). IR (Nujol) cm^{-1}: 1655, 1525, 1430. Anal. ($C_{25}H_{21}N_7O$) C, H, N.

2-[Ethyl-(2-furan-2-yl-8-methyl-8H-pyrazolo[4,3-e][1,2,4]triazolo-[1,5-c]pyrimidin-5-yl)amino]ethanol (**58**). Yield 88%; pale yellow solid (EtOAc/petroleum ether) mp 183 °C; ^{1}H NMR ($CDCl_3$) δ: 1.32 (3H, t, J = 7), 3.53−3.62 (4H, m), 3.88 (3H, s), 4.62 (2H, t, J = 8), 6.51 (1H, dd, J = 2, J = 4), 7.03 (1H, d, J = 4), 7.53 (1H, d, J = 2), 8.00 (1H, s). IR (Nujol) cm^{-1}: 3450−3110, 1625, 1535, 1425. Anal. ($C_{15}H_{17}N_7O_2$) C, H, N.

2-Furan-2-yl-8-methyl-5-pyrrolidin-1-yl-8H-pyrazolo[4,3-e]-[1,2,4]triazolo[1,5-c]pyrimidine (**59**). Yield 91%; pale yellow solid (EtOAc/petroleum ether) mp 270 °C; ^{1}H NMR ($CDCl_3$) δ: 2.03 (4H, bs), 4.03−4.12 (7H, m), 6.57 (1H, dd, J = 2, J = 4), 7.18 (1H, d, J = 4), 7.61 (1H, d, J = 2), 8.06 (1H, s). IR (Nujol) cm^{-1}: 1630, 1515, 1420. Anal. ($C_{15}H_{15}N_7O$) C, H, N.

2-Furan-2-yl-8-methyl-5-piperidin-1-yl-8H-pyrazolo[4,3-e][1,2,4]-triazolo[1,5-c]pyrimidine (**60**). Yield 89%; pale yellow solid (EtOAc/petroleum ether) mp 181 °C; ^{1}H NMR ($CDCl_3$) δ: 1.76 (6H, bs), 3.92−3.95 (4H, m), 4.13 (3H, s), 6.58 (1H, dd, J = 2, J = 4), 7.22 (1H, d, J = 4), 7.62 (1H, d, J = 2), 8.14 (1H, s). IR (Nujol) cm^{-1}: 1640, 1525, 1405. Anal. ($C_{16}H_{17}N_7O$) C, H, N.

2-Furan-2-yl-8-methyl-5-(4-methyl-piperazin-1-yl)-8H-pyrazolo-[4,3-e][1,2,4]triazolo[1,5-c]pyrimidine (**61**). Yield 76%; pale yellow solid (EtOAc/petroleum ether) mp 221 °C; ^{1}H NMR ($CDCl_3$) δ: 2.56 (3H, s), 2.81−3.03 (4H, m), 4.15−4.33 (7H, m), 6.58 (1H, dd, J = 2, J = 4), 7.19 (1H, d, J = 4), 7.62 (1H, d, J = 2), 8.14 (1H, s). IR (Nujol) cm^{-1}: 1625, 1530, 1415. Anal. ($C_{16}H_{18}N_8O$) C, H, N.

2-Furan-2-yl-8-methyl-5-morpholin-4-yl-8H-pyrazolo[4,3-e]-[1,2,4]triazolo[1,5-c]pyrimidine (**62**). Yield 93%; pale orange solid (EtOAc/petroleum ether) mp 246 °C; ^{1}H NMR ($CDCl_3$) δ: 3.94−4.05 (8H, m), 4.14 (3H, s), 6.58 (1H, dd, J = 2, J = 4), 7.22 (1H, d, J = 4), 7.63 (1H, d, J = 2), 8.17 (1H, s). IR (Nujol) cm^{-1}: 1630, 1525, 1430. Anal. ($C_{15}H_{15}N_7O_2$) C, H, N.

B. Biological Activity. Binding at Human A_1, A_{2A}, and A_3 Adenosine Receptors. All pharmacological methods followed the procedures as described earlier.[30] In brief, membranes for radioligand binding were prepared from CHO cells stably transfected with human adenosine receptor subtypes in a two-step procedure. In a first low-speed step (1000g) cell fragments and nuclei were removed. The crude membrane fraction was sedimented from the supernatant at 100 000g. The membrane pellet was resuspended in the buffer used for the respective binding experiments, frozen in liquid nitrogen, and stored at 80 °C. For the measurement of adenylyl cyclase activity, only one high speed centrifugation of the homogenate was used. The resulting crude membrane pellet was resuspended in 50 mM Tris/HCl, pH 7.4, and immediately used for the cyclase assay.

For radioligand binding at A_1 adenosine receptors, 1 nM [^{3}H]CCPA was used, whereas 30 and 10 nM [^{3}H]NECA were used for A_{2A} and A_3 receptors, respectively. Nonspecific binding of [^{3}H]CCPA was determined in the presence of 1 mM theophylline, and in the case of [^{3}H]NECA 100 μM R-PIA was used.[38]

Adenylyl Cyclase Activity. The potency of antagonists at the A_{2B} receptor was determined in adenylyl cyclase experiments. The procedure was carried out as described previously with minor modifications.[30,39] Membranes were incubated with about 150 000 cpm of [α-^{32}P]ATP for 20 min in the incubation mixture as described without EDTA and NaCl.[39,40] For agonists, the EC_{50} values for the stimulation of adenylyl cyclase were calculated with the Hill equation. Hill coefficients in all experiments were near unity. IC_{50} values for concentration-dependent inhibition of NECA-stimulated adenylyl cyclase caused by antagonists was calculated accordingly. Dissociation

dx.doi.org/10.1021/jm300899q | J. Med. Chem. 2012, 55, 9654−9668

constants (K_i) for antagonists were then calculated with the Cheng and Prusoff equation.[40]

C. Molecular Modeling. Modeling studies were carried out on a 20 CPU (Intel Core2 Quad CPU 2.40 GHz) Linux cluster. Energy calculations and analyses of docking poses were performed with the Molecular Operating Environment (MOE, version 2010.10) suite.[41] Quantum mechanical calculations were carried out with the software package MOPAC (version 7), as implemented in MOE.[42] Gold suite (version 5.0) was used to perform all the docking simulations.[43]

Three Dimensional Structures of hA_{2A} AR, and hA_3 AR. The crystallographic structure of hA_{2A} AR, in complex with the high affinity antagonist ZM241385 (PDB access code: 3EML),[32] and a previously reported homology model of the hA_3 AR[31] were used to perform molecular docking studies at these receptor subtypes. The numbering of the amino acids follows the arbitrary scheme by Ballesteros and Weinstein: each amino acid identifier starts with the helix number, followed by the position relative to a reference residue among the most conserved amino acids in that helix, to which the number 50 is arbitrarily assigned.[44]

Molecular Docking of hA_3 AR Antagonists. Ligand structures were built using the MOE-builder tool, as part of the MOE suite,[41] and were subjected to a MMFF94x energy minimization until the rms conjugate gradient was <0.05 kcal mol^{-1} $Å^{-1}$. The validation of the proposed docking protocol has been previously published.[45]

All antagonists were docked into the hypothetical TM binding site of the hA_3 AR model and the orthosteric binding site of the hA_{2A} AR crystal structure, by employing the docking tool of the GOLD suite.[43] For each compound, 25 independent docking runs were performed and searching was conducted within a user-specified docking sphere with the Genetic Algorithm protocol and the GoldScore scoring function. The resulting docking complexes (ligand and side-chain residues within 4.5 Å) were subjected to a MMFF94x energy minimization until the rms conjugate gradient was <1 kcal mol^{-1} $Å^{-1}$.

Prediction of antagonist−receptor complex stability (in terms of corresponding pK_i value) and the quantitative analysis for nonbonded intermolecular interactions (H-bonds, transition metals, water bridges, hydrophobic, electrostatic) were calculated and visualized using several tools implemented in the MOE suite.[41] Electrostatic and hydrophobic contributions to the binding energy of individual amino acids have been calculated with MOE.[41] To estimate the electrostatic contributions, atomic charges for the ligands were calculated with MOPAC[42] and the PM3/ESP methodology, whereas partial charges for the protein amino acids were computed with the AMBER99 force field.

Molecular Dynamics. Each ligand−protein complex was embedded in a 1-palmitoyl-2-oleoyl-*sn*-glycero-3-phosphocholine (POPC) lipid bilayer (75 × 75 Å wide) and placed into the membrane according to the suggested orientation reported in the "Orientations of Proteins in Membranes (OPM)" database[46] for the hA_{2A} AR. The so-obtained membrane−receptor complexes were solvated with TIP3P[47] water using the program Solvate 1.0[48] and neutralized by Na^+/Cl^- counterions to a final concentration of 0.154 M. Membrane molecular dynamics simulations were carried out on a GPU cluster with the ACEMD program[49] using the CHARMM27 force field[50] and periodic boundaries conditions. Initial parameters for the ligands were derived from the CHARMM general force field for organic molecules[51] by using the paramchem service[52] and were subsequently optimized at the MP2/6-31G* level of theory[53] (consistently with the CHARMM27 force field parametrization) by using Gaussian 09[54] and the implemented parametrization tools in the VMD engine.[55]

The system was equilibrated using a stepwise procedure: In the first stage, to reduce steric clashes due to the manual setting up of the membrane−receptor system, a 500-steps conjugate-gradient minimization was performed. Then, to allow lipids to reach equilibrium and water molecules to diffuse into the protein cavity, the system was equilibrated by keeping the positions of protein and ligand atoms restrained for the first 8 ns by a force constant of 1 kcal/mol·$Å^2$ and then by keeping only the α carbon atoms frozen up to 9 ns while gradually reducing the force constant to 0.1 kcal/mol·$Å^2$. During the equilibration procedure, the temperature was maintained at 298 K using a Langevin thermostat with a low damping constant of 1 ps^{-1}, and the pressure was maintained at 1 atm using a Berendensen barostat. Bond lengths involving hydrogen atoms were constrained using the M-SHAKE[56] algorithm with an integration time step of 2 fs.

Harmonical constraints were then removed during the 60 ns of the NVT ensemble. Long-range Coulomb interactions were handled using the particle mesh Ewald summation method (PME)[57] with grid size rounded to the approximate integer value of cell wall dimensions. A nonbonded cutoff distance of 9 Å with a switching distance of 7.5 Å was used.

■ ASSOCIATED CONTENT

Ⓢ Supporting Information

Elemental analyses and additional modeling figures and videos. This material is available free of charge via the Internet at http://pubs.acs.org.

■ AUTHOR INFORMATION

Corresponding Author

*Tel +39 040 5583726 (G.S.), +39 049 8275704 (S.M.). Fax +39 040 52572 (G.S.), +39 049 8275366 (S.M.). E-mail: spalluto@units.it (G.S.); stefano.moro@unipd.it (S.M.).

Notes

The authors declare no competing financial interest.

■ ACKNOWLEDGMENTS

The work was supported by a grant from the Italian Ministry for University and Research (MIUR, FIRB RBNE03YA3L project). The molecular modeling work coordinated by S.M. has been carried out also with financial support from the University of Padova, Italy. S.M. is also very grateful to Chemical Computing Group and Acellera for the scientific and technical partnership.

■ ABBREVIATIONS USED

AR, adenosine receptor; ATP, adenosine triphosphate; BM, binding mode; CHO, Chinese hamster ovary; DMSO, dimethyl sulfoxide; EDTA, ethylenediaminetetraacetic acid; GPCR, G protein-coupled receptor; [^{3}H]-CCPA, [^{3}H]-2-chloro-6-cyclopentyladenosine; IEFs, interaction energy fingerprints; MD, molecular dynamics; NECA, 5′-*N*-ethylcarboxamidoadenosine; POPC, 1-palmitoyl-2-oleoyl-*sn*-glycero-3-phosphocholine; PTP, pyrazolo[4,3-*e*]1,2,4-triazolo[1,5-*c*]pyrimidine; *R*-PIA, *R*-N^6-phenylisopropyladenosine; TLC, thin layer chromatography; ZM241385, 4-[2-[7-amino-2-(2-furyl)-1,2,4-triazolo[1,5-*a*][1,3,5]triazin-5-yl-amino]ethylphenol; SAR, structure−activity relationship; TM, transmembrane; EL2, second extracellular loop

■ REFERENCES

(1) Fredholm, B. B.; IJzerman, A. P.; Jacobson, K. A.; Klotz, K. N.; Linden, J. International Union of Pharmacology. XXV. Nomenclature and classification of adenosine receptors. *Pharmacol. Rev.* **2001**, *53*, 527−552.

(2) Fredholm, B. B.; Arslan, G.; Halldner, L.; Kull, B.; Schulte, G.; Wasserman, W. Structure and function of adenosine receptors and their genes. *Naunyn-Schmiedeberg's Arch. Pharmacol.* **2000**, *362*, 364−374.

(3) Meyerhof, W.; Muller-Brechlin, R.; Richter, D. Molecular cloning of a novel putative G-protein coupled receptor expressed during rat spermiogenesis. *FEBS Lett.* **1991**, *284*, 155−160.

(4) Sajjadi, F. G.; Firestein, G. S. cDNA cloning and sequence analysis of the human A_3 adenosine receptor. *Biochim. Biophys. Acta* **1993**, *1179*, 105−107.

(5) Salvatore, C. A.; Jacobson, M. A.; Taylor, H. E.; Linden, J.; Johnson, R. G. Molecular cloning and characterization of the human A_3 adenosine receptor. *Proc. Natl. Acad. Sci. U.S.A.* **1993**, *90*, 10365−10369.
(6) Linden, J. Cloned adenosine A_3 receptors: Pharmacological properties, species differences and receptor functions. *Trends Pharmacol. Sci.* **1994**, *15*, 298−306.
(7) Zhao, Z. H.; Ravid, S.; Ravid, K. Chromosomal mapping of the mouse A_3 adenosine receptor gene, adora3. *Genomics* **1995**, *30*, 118−119.
(8) Hill, R. J.; Oleynek, J. J.; Hoth, C. F.; Kiron, M. A.; Weng, W. F.; Wester, R. T.; Tracey, W. R.; Knight, D. R.; Buchholz, R.; Kennedy, S. P. Cloning, expression and pharmacological characterization of rabbit A_1 and A_3 receptors. *J. Pharmacol. Exp. Ther.* **1997**, *280*, 122−128.
(9) Linden, J.; Taylor, H. E.; Robeva, A. S.; Tucker, A. L.; Stehle, J.; Rivkees, S. A.; Fink, J. S.; Reppert, S. M. Molecular cloning and functional expression of a sheep A_3 adenosine receptor with widespread tissue distribution. *Mol. Pharmacol.* **1993**, *44*, 524−532.
(10) Hannon, J. P.; Pfannkuche, H. J.; Fozard, J. R. A role for mast cells in adenosine A_3 receptor-mediated hypotension in the rat. *Br. J. Pharmacol.* **1995**, *115*, 945−952.
(11) Varani, K.; Cacciari, B.; Baraldi, P. G.; Dionisotti, S.; Borea, P. A. Binding affinity of adenosine receptor agonists and antagonists at human cloned A_3 adenosine receptors. *Life Sci.* **1998**, *63*, 81−87.
(12) Jacobson, K. A. Adenosine A_3 receptors: novel ligands and paradoxical effects. *Trends Pharmacol. Sci.* **1998**, *19*, 184−191.
(13) Abbracchio, M. P.; Brambilla, R.; Kim, H. O.; von Lubitz, D. K. J.; Jacobson, K. A.; Cattabeni, F. G-protein-dependent activation of phospholipase-C by adenosine A_3 receptor in rat brain. *Mol. Pharmacol.* **1995**, *48*, 1038−1045.
(14) Jacobson, K. A.; Suzuki, F. Recent developments in selective agonists and antagonists acting at purine and pyrimidine receptors. *Drug. Dev. Res.* **1996**, *39*, 289−300.
(15) van Schaick, E. A.; Jacobson, K. A.; Kim, H. O.; IJzerman, A. P.; Danhof, M. Haemodynamic effects and histamine release elicited by the selective adenosine A_3 receptor agonists 2-Cl-IB-MECA in conscious rats. *Eur. J. Pharmacol.* **1996**, *308*, 311−314.
(16) von Lubitz, D. K. J.; Carter, M. F.; Deutsch, S. I.; Lin, R. C. S.; Mastropaolo, J.; Meshulam, J.; Jacobson, K. A. The effects of adenosine A_3 receptor stimulation on seizures in mice. *Eur. J. Pharmacol.* **1995**, *275*, 23−29.
(17) Mackenzie, W. M.; Hoskin, D. W.; Blay, J. Adenosine inhibits the adhesion of anti-CD3-activated killer lymphocytes to adenocarcinoma cells through an A_3 receptor. *Cancer Res.* **1994**, *54*, 3521−3526.
(18) Brambilla, R.; Cattabeni, F.; Ceruti, S.; Barbieri, D.; Franceschi, C.; Kim, Y.; Jacobson, K. A.; Klotz, K. N.; Lohse, M. J.; Abbracchio, M. P. Activation of the A_3 adenosine receptor effects cell cycle progression and cell growth. *Naunyn-Schmiedeberg's Arch. Pharmacol.* **2000**, *361*, 225−234.
(19) Forsythe, P.; Ennis, M. Adenosine, mast cells and asthma. *Inflammation Res.* **1999**, *48*, 301−307.
(20) Ramkumar, V.; Stiles, G. L.; Beaven, M. A.; Ali, H. The A_3 adenosine receptor is the unique adenosine receptor which facilitates release of allergic mediators in mast cells. *J. Biol. Chem.* **1993**, *268*, 16887−16890.
(21) Jacobson, K. A.; Gao, Z. G. Adenosine receptors as therapeutic targets. *Nat. Rev. Drug Discovery* **2006**, *5*, 247−264.
(22) Moro, S.; Gao, Z. G.; Jacobson, K. A.; Spalluto, G. Progress in the pursuit of therapeutic adenosine receptor antagonists. *Med. Res. Rev.* **2006**, *26*, 131−159.
(23) Baraldi, P. G.; Cacciari, B.; Romagnoli, R.; Spalluto, G.; Klotz, K. N.; Leung, E.; Varani, K.; Gessi, S.; Merighi, S.; Borea, P. A. Pyrazolo[4,3-*e*]1,2,4-triazolo[1,5-*c*]pyrimidine derivatives as highly potent and selective human A_3 adenosine receptor antagonists. *J. Med. Chem.* **1999**, *42*, 4473−4478.
(24) Baraldi, P. G.; Cacciari, B.; Romagnoli, R.; Spalluto, G.; Moro, S.; Klotz, K. N.; Leung, E.; Varani, K.; Gessi, S.; Merighi, S.; Borea, P. A. Pyrazolo[4,3-*e*]1,2,4-triazolo[1,5-*c*]pyrimidine derivatives as highly potent and selective human A_3 adenosine receptor antagonists: Influence of the chain at N^8 pyrazole nitrogen. *J. Med. Chem.* **2000**, *43*, 4768−4780.
(25) Baraldi, P. G.; Cacciari, B.; Moro, S.; Spalluto, G.; Pastorin, G.; Da Ros, T.; Klotz, K. N.; Varani, K.; Gessi, S.; Borea, P. A. Synthesis, biological activity, and molecular modeling investigation of new pyrazolo[4,3-*e*]1,2,4-triazolo[1,5-*c*]pyrimidine derivatives as human A_3 adenosine receptor antagonists. *J. Med. Chem.* **2002**, *45*, 770−780.
(26) Maconi, A.; Pastorin, G.; Da Ros, T.; Spalluto, G.; Gao, Z. G.; Jacobson, K. A.; Baraldi, P. G.; Cacciari, B.; Varani, K.; Borea, P. A. Synthesis, biological properties and molecular modeling investigation of the first potent, selective and water soluble human A_3 adenosine receptor antagonist. *J. Med. Chem.* **2002**, *45*, 3579−3582.
(27) Pastorin, G.; Da Ros, T.; Bolcato, C.; Montopoli, C.; Moro, S.; Cacciari, B.; Baraldi, P. G.; Varani, K.; Borea, P. A.; Spalluto, G. Synthesis and biological studies of a new series of 5-heteroarylcarbamoylamino-pyrazolo[4,3-*e*]1,2,4triazolo[1,5-*c*]pyrimidines as human A_3 adenosine receptor antagonists. Influence of the heteroaryl substituent on binding affinity and molecular modeling investigation. *J. Med. Chem.* **2006**, *49*, 1720−1729.
(28) Cheong, S. L.; Dolzhenko, A.; Kachler, S.; Paoletta, S.; Federico, S.; Cacciari, B.; Dolzhenko, A.; Klotz, K. N.; Moro, S.; Spalluto, G.; Pastorin, G. The significance of 2-furyl substitutions with a 2-(para-substituted) aryl group in a new series of pyrazolo-triazolo-pyrimidines as potent and highly selective hA_3 adenosine receptor antagonists: new insight into structure−activity relationship and receptor antagonist recognition. *J. Med. Chem.* **2010**, *53*, 3361−3375.
(29) Kozma, E.; Kumar, T. S.; Federico, S.; Phan, K.; Balasubramanian, R.; Gao, Z. G.; Paoletta, S.; Moro, S.; Spalluto, G.; Jacobson, K. A. Novel fluorescent antagonist as a molecular probe in A_3 adenosine receptor binding assays using flow cytometry. *Biochem. Pharmacol.* **2012**, *83*, 1552−1561.
(30) Klotz, K. N.; Hessling, J.; Hegler, J.; Owman, C.; Kull, B.; Fredholm, B. B.; Lohse, M. J. Comparative pharmacology of human adenosine receptor subtypes - characterization of stably transfected receptors in CHO cells. *Naunyn-Schmiedeberg's Arch. Pharmacol.* **1998**, *357*, 1−9.
(31) Lenzi, O.; Colotta, V.; Catarzi, D.; Varano, F.; Poli, D.; Filacchioni, G.; Varani, K.; Vincenzi, F.; Borea, P. A.; Paoletta, S.; Morizzo, E.; Moro, S. 2-Phenylpyrazolo[4,3-*d*]pyrimidin-7-one as a new scaffold to obtain potent and selective human A_3 adenosine receptor antagonists: new insights into the receptor-antagonist recognition. *J. Med. Chem.* **2009**, *52*, 7640−7652.
(32) Jaakola, V. P.; Griffith, M. T.; Hanson, M. A.; Cherezov, V.; Chien, E. Y. T.; Lane, J. R.; IJzerman, A. P.; Stevens, R. C. The 2.6 angstrom crystal structure of a human A_{2A} adenosine receptor bound to an antagonist. *Science* **2008**, *322*, 1211−1217.
(33) Kim, J.; Wess, J.; van Rhee, M.; Schoneberg, T.; Jacobson, K. A. Site-directed mutagenesis identifies residues involved in ligand recognition in the human A_{2A} adenosine receptor. *J. Biol. Chem.* **1995**, *270*, 13987−13997.
(34) Gao, Z. G.; Chen, A.; Barak, D.; Kim, S. K.; Muller, C. E.; Jacobson, K. A. Identification by site-directed mutagenesis of residues involved in ligand recognition and activation of the human A_3 adenosine receptor. *J. Biol. Chem.* **2002**, *277*, 19056−19063.
(35) Congreve, M.; Andrews, S. P.; Doré, A. S.; Hollenstein, K.; Hurrell, E.; Langmead, C. J.; Mason, J. S.; Ng, I. W.; Tehan, B.; Zhukov, A.; Weir, M.; Marshall, F. H. Discovery of 1,2,4-triazine derivatives as adenosine A_{2A} antagonists using structure-based drug design. *J. Med. Chem.* **2012**, *55*, 1898−1903.
(36) Sabbadin, D.; Ciancetta, A.; Moro, S. Bridging molecular docking to membrane molecular dynamics to investigate GPCR−ligand recognition: the human A_{2A} adenosine receptor as a key study. *J. Am. Chem. Soc.* **2012**, submitted.
(37) Mason, J. S.; Bortolato, A.; Congreve, M.; Marshall, F. H. New insights from structural biology into the druggability of G protein-coupled receptors. *Trends Pharmacol. Sci.* **2012**, *33*, 249−260.
(38) De Lean, A.; Hancock, A. A.; Lefkowitz, R. J. Validation and statistical analysis of a computer modeling method for quantitative

analysis of radioligand binding data for mixtures of pharmacological receptor subtypes. *Mol. Pharmacol.* **1982**, *21*, 5−16.
(39) Klotz, K. N.; Cristalli, G.; Grifantini, M.; Vittori, S.; Lohse, M. J. Photoaffinity labeling of A_1 adenosine receptors. *J. Biol. Chem.* **1985**, *260*, 14659−14664.
(40) Cheng, Y. C.; Prusoff, H. R. Relationships between the inhibition constant (K_i) and the concentration of inhibitor which causes 50% inhibition (IC_{50}) of an enzymatic reaction. *Biochem. Pharmacol.* **1973**, *22*, 3099−3108.
(41) *MOE (Molecular Operating Environment)*, version 2010.10; Chemical Computing Group Inc., 1010 Sherbooke St. West, Suite #910, Montreal, Quebec, Canada, 2010.
(42) Stewart, J. J. P. *MOPAC 7*; Fujitsu Limited, Tokyo, Japan, 1993.
(43) *GOLD suite*, version 1.3.2; Cambridge Crystallographic Data Centre, Cambridge.
(44) Ballesteros, J. A.; Weinstein, H. Integrated methods for the construction of three dimensional models and computational probing of structure-function relationships in G-protein coupled receptors. *Methods Neurosci.* **1995**, *25*, 366−428.
(45) Cheong, S. L.; Dolzhenko, A. V.; Paoletta, S.; Lee, E. P. R.; Kachler, S.; Federico, S.; Klotz, K.-N.; Dolzhenko, A. V.; Spalluto, G.; Moro, S.; Pastorin, G. Does the combination of optimal substitutions at the C^2-, N^5- and N^8-positions of the pyrazolo-triazolo-pyrimidine scaffold guarantee selective modulation of the human A_3 adenosine receptors? *Bioorg. Med. Chem.* **2011**, *19*, 6120−6134.
(46) Lomize, M. A.; Lomize, A. L.; Pogozheva, I. D.; Mosberg, H. I. OPM: orientations of proteins in membranes database. *Bioinformatics* **2006**, *22*, 623−625.
(47) Jorgensen, W. L.; Chandrasekhar, J.; Madura, J. D.; Impey, R. W.; Klein, M. L. Comparison of simple potential functions for simulating liquid water. *J. Chem. Phys.* **1983**, *79*, 926−935.
(48) Grubmüller, H; Groll,V. Solvate v 1.0 available at http://www.mpibpc.mpg.de/home/grubmueller/downloads/solvate/index.html.
(49) Harvey, M. J.; Giupponi, G.; Fabritiis, G. D. ACEMD: Accelerating biomolecular dynamics in the microsecond time scale. *J. Chem. Theory Comput.* **2009**, *5*, 1632−1639.
(50) MacKerell, A. D., Jr.; Banavali, N.; Foloppe, N. Development and current status of the CHARMM force field for nucleic acids. *Biopolymers* **2001**, *56*, 257−265.
(51) Vanommeslaeghe, K.; Hatcher, E.; Acharya, C.; Kundu, S.; Zhong, S.; Shim, J.; Darian, E.; Guvench, O.; Lopes, P.; Vorobyov, I.; MacKerell, A. D., Jr. CHARMM general force field: A force field for drug-like molecules compatible with the CHARMM all-atom additive biological force fields. *J. Comput. Chem.* **2010**, *31*, 671−690.
(52) www.paramchem.org.
(53) Head-Gordon, M.; Pople, J. A.; Frisch, M. J. MP2 Energy Evaluation by Direct Methods. *Chem. Phys. Lett.* **1988**, *153*, 503−506.
(54) Frisch, M. J.; Trucks, G. W.; Schlegel, H. B.; Scuseria, G. E.; Robb, M. A.; Cheeseman, J. R.; Scalmani, G.; Barone, V.; Mennucci, B.; Petersson, G. A.; Nakatsuji, H.; Caricato, M.; Li, X.; Hratchian, H. P.; Izmaylov, A. F.; Bloino, J.; Zheng, G.; Sonnenberg, J. L.; Hada, M.; Ehara, M.; Toyota, K.; Fukuda, R.; Hasegawa, J.; Ishida, M.; Nakajima, T.; Honda, Y.; Kitao, O.; Nakai, H.; Vreven, T.; Montgomery, J. A., Jr.; Peralta, J. E.; Ogliaro, F.; Bearpark, M.; Heyd, J. J.; Brothers, E.; Kudin, K. N.; Staroverov, V. N.; Kobayashi, R.; Normand, J.; Raghavachari, K.; Rendell, A.; Burant, J. C.; Iyengar, S. S.; Tomasi, J.; Cossi, M.; Rega, N.; Millam, N. J.; Klene, M.; Knox, J. E.; Cross, J. B.; Bakken, V.; Adamo, C.; Jaramillo, J.; Gomperts, R.; Stratmann, R. E.; Yazyev, O.; Austin, A. J.; Cammi, R.; Pomelli, C.; Ochterski, J. W.; Martin, R. L.; Morokuma, K.; Zakrzewski, V. G.; Voth, G. A.; Salvador, P.; Dannenberg, J. J.; Dapprich, S.; Daniels, A. D.; Farkas, Ö.; Foresman, J. B.; Ortiz, J. V.; Cioslowski, J.; Fox, D. J. *Gaussian 09*, revision B.01; Gaussian Inc., Wallingford, CT, 2009.
(55) Humphrey, W.; Dalke, A.; Schulten, K. VMD: visual molecular dynamics. *J. Mol. Graph.* **1996**, *14*, 33−38.
(56) Krautler, V.; Van Gunsteren, W. F.; Hunenberger, P. H. A fast SHAKE algorithm to solve distance constraint equations for small molecules in molecular dynamics simulations. *J. Comput. Chem.* **2001**, *22*, 501−508.
(57) Essmann, U.; Perera, L.; Berkowitz, M. L.; Darden, T.; Lee, H.; Pedersen, L. G. A smooth particle mesh Ewald method. *J. Chem. Phys.* **1995**, *103*, 8577−8593.